AVIAN-INSPIRED PASSIVE LANDING MECHANISMS FOR PERCHING ROTORCRAFT

by

Courtney E. Doyle

A thesis submitted to the faculty of
The University of Utah
in partial fulfillment of the requirements for the degree of

Master of Science

Department of Mechanical Engineering

The University of Utah

December 2011

The University of Utah Graduate School

STATEMENT OF THESIS APPROVAL

The thesis of **Courtney E. Doyle**

has been approved by the following supervisory committee members:

Mark A. Minor	, Chair	**10/25/2011** Date Approved
Jake J. Abbott	, Member	**10/25/2011** Date Approved
Sanford G. Meek	, Member	**10/27/2011** Date Approved

and by **Timothy A. Ameel** , Chair of the Department of **Mechanical Engineering**

and by Charles A. Wight, Dean of The Graduate School.

ABSTRACT

Autonomous and teleoperated flying robots capable of perch-and-stare are desirable for reconnaissance missions. Current solutions for perch-and-stare applications utilize various methods to enable aircraft to land on a limited set of surfaces that are typically horizontal or vertical planes. Motivated by the fact that songbirds are able to sleep in trees, without requiring active muscle control to stay perched, the research presented here details a concept that allows for passive perching of rotorcraft on a variety of surfaces.

This thesis presents two prototype iterations, where perching is accomplished through the integration of two components: a compliant, underactuated gripping foot and a collapsing leg mechanism that converts aircraft weight into tendon tension in order to passively actuate the foot. This thesis presents the design process and analysis of the mechanisms. Additionally, stability tests were performed on the second prototype, attached to a quadrotor, that detail the versatility of the system and ability of the system to support external moments. The results show promise that it is possible to passively perch a rotorcraft on multiple surfaces and support reasonable environmental disturbances.

CONTENTS

LIST OF FIGURES

LIST OF TABLES

ACKNOWLEDGMENTS

First, I would like to thank my advisors Dr. Mark Minor and Dr. Jake Abbott for their support and mentoring through the development of this work. I would also like to recognize the manufacturing work of Taylor Isom and the design efforts of the rest of the Bio-Inspired Graspers senior design team (Justin Bird, Christopher Johnson, Jason Kallman, and Jason Simpson), as well as Raymond King. Finally, I would like to thank my friends and family who supported me and helped keep me motivated, especially during the final months.

CHAPTER 1

INTRODUCTION

Perch-and-stare describes a maneuver in which a robot flies to a vantage point and lands to collect intelligence. A flying robot capable of perch-and-stare, equipped with cameras and other sensors, can provide an inconspicuous reconnaissance platform. Additionally, robot perching provides a potential mechanism for recharging the robot's power source (e.g., through the use of photovoltaics).

It is desirable for perch-and-stare applications that a robot be able to land on a variety of surfaces. Inspired by the adaptability of songbirds, this research aims to design a landing mechanism capable of perching on curved surfaces. The design is developed with the intention of being attached to an autonomous rotorcraft capable of vertical take-off and landing, similar to a bird's transition into a hover-like maneuver when perching, Fig. 1.1.

As a basis for the development of our design, a literature review was performed focusing on four topics: autonomous perching robots, unmanned areal vehicles, functional anatomy specific to songbirds, and underactuated grippers. Relevant research for each topic is presented in the following sections.

1.1 Autonomous Perching Robots

The practicality of reliable robot perching is recognized, and a number of research groups are pursuing solutions using a variety of methods. This section summarizes recent projects, which include robots that land on horizontal, vertical, and string-type surfaces. Each of these methods

Figure 1.1. Conceptual drawing of perching mechanism. Through the use of clever mechanism design, a rotorcraft (e.g., helicopter) can passively perch on a curved surface, similar to a bird.

is limited by the landing surface required for successful perching; the goal of our avian-inspired approach is to offer more versatility.

Researchers at MIT have developed a method to perform a high-speed maneuver with a fixed-wing robot, such that the robot pulls up into a high angle-of-attack to perch on a suspended string via a latching hook [1]. Their work is inspired by the perching maneuver performed by birds, however it only addresses the flight maneuverability rather than perch versatility.

Researchers at Stanford University have used a high angle-of-attack approach to attach a fixed-wing robot to a vertical surface [2]. Again, much of their inspiration derives from birds, as well as other flying animals, but is mostly focused on flight patterns and maneuvers. Microspine technology is incorporated to allow for successful adhesion to the vertical walls.

Researchers at the University of Pennsylvania have similarly attached spines to a quadrotor [3]. Their simultaneous control work with quadrotors allowed them to develop a system that can successfully attach to flat surfaces at various angles.

Researchers at Cornell University are incorporating a morphing structure inspired by the wings and tail of a bird during landing [4, 5]. Their work proposes that the ability to change shape in flight will provide practical perching maneuvers for perching robots. A subsequent perching mechanism is not presented.

Researchers at the University of Florida, and colleagues, developed a winged robot with crawling legs, designed to land on a relatively large target zone, and then use its legs to crawl [6, 7]. This technology is adaptable to the mission of perch-and-stare as the robot can land on a flat surface, such as a rooftop, and crawl to the edge for reconnaissance.

1.2 Unmanned Aerial Vehicles (UAV)

The intent of our design is to be attached to a rotorcraft capable of autonomous flight; as such it is important to present a summary of current capabilities in autonomous maneuverability. This section provides a brief description of current research with UAVs.

Numerous computer science researchers have been applying concepts of machine learning and artificial intelligence to teach helicopters and other rotorcraft to complete complex aerial maneuvers. One particularly active group at Stanford has applied numerous techniques to accomplish difficult flight acrobatics with helicopters [8]. Researchers at the University of Pennsylvania have developed control algorithms for a quadrotor that allow for aggressive maneuvers such as flying through tight spaces and perching, though it requires use of an external vision system [9].

In addition to completing autonomous aerial maneuvers, research has been conducted on autonomous navigation. Researchers at Drexel University equipped a miniature rotorcraft with optic-flow and ultrasonic sensors, enabling the robot to find and land on the edge of buildings

[10]. Researchers at MIT have explored methods for autonomous navigation without GPS using an on-board camera [11].

1.3 Songbird Functional Anatomy

There are a number of adaptations unique to songbirds (Order Passeriformes), and some other tree-dwelling birds, that make them efficient at perching on a variety of surfaces. This section discusses two points of interest: foot structure and tendon routing.

For songbirds, foot and leg anatomy is important for perching functionality [13]. Most songbirds have an anisodactyl toe arrangement, Fig. 1.2(a), with three forward facing toes and one backward facing toe. In addition, birds' feet are underactuated, meaning they have more degrees of freedom than muscles to control them. This feature enables the feet to passively conform to the structure on which they are attempting to perch.

Additionally, songbirds exhibit a particulary interesting adaptation that equips them for life in the trees [13, 14]. As shown in Fig. 1.2(b), songbirds have a tendon on the rear side of the ankle that automatically causes the toes to grip around a branch when the leg bends. This tendon enables songbirds to sleep while perching without active control of gripping. As a bird relaxes, the weight of its body causes the legs to bend and the toes to grip; deeper relaxation leads to a tighter grip. When the bird is ready to take off, it must actively stand up to let go of the perch. This anatomy is key to the development of our passively actuated system; the weight of the rotorcraft is used to actuate the gripping mechanism; when the rotorcraft lifts off, the foot will naturally release.

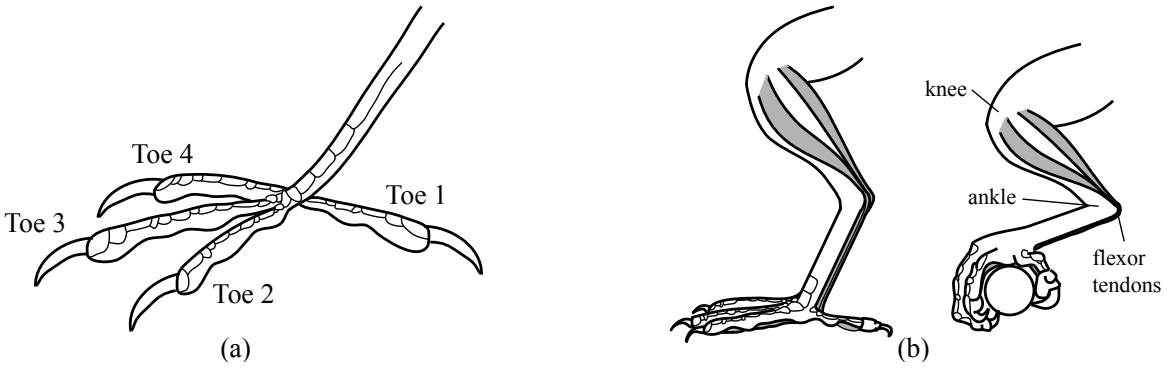

Figure 1.2. Songbird foot and leg anatomy. (a) Songbirds exhibit an anisodactyl toe arrangement with three toes in front and one toe in back. (b) Songbirds have evolved a useful adaptation that allows for sleeping while perching. As the bird folds it legs, the tendons on the rear side of the ankle automatically grip the toes around the branch. This enables the relaxed leg of a sleeping bird to tightly grip the perch without any voluntary muscle effort. Figure recreated based on an image in [12].

1.4 Underactuated Grippers

To date, a single study has investigated robot gripping inspired by the foot of a bird. Researchers at Clemson University analyzed the feet of raptors, motivated by their excellent stable grasping ability and simple design relative to anthropomorphic hands [15]. They went on to design a non-anthropomorphic "thumbless" grasping hand reminiscent of a raptor foot [16]; most of the joints have independent actuation.

A number of research groups have, however, studied and designed underactuated grippers, and similar methods can be implemented for our landing gear. In general, underactuated grippers can be grouped into categories based on their force transmission; the two most common systems utilize either cable-based transmission or linkage-based transmission, while a few groups have explored more unique solutions.

Perhaps the largest category of underactuated hands are those of cable-driven systems, which are attractive to this research due to the similarities with the tendon based appendages found in nature. Due to the number of groups developing designs, the collection of cable-driven systems is fairly diverse. One of the earliest systems was developed by Hirose and Umetani consisting of a multi-link, two-fingered mechanism driven by a pair of wires (flexor and extensor) wrapped around successively smaller pulleys [17]. A similar design was used at Northeastern University to develop Graspar, a three-fingered hand capable of grasping a variety of objects [18]. Other groups have employed a single tendon for flexing while utilizing springs for a restoring force [19, 20, 21]; the group at Université Laval is capable of controlling a 15-dof hand with a single motor [19]. Of particular interest to us is an underactuated design of Dollar and Howe in which an 8-dof four-fingered hand is controlled using a single actuator [22]. Their design uses compliant joints between stiff link segments with a cable secured at the distal links to transmit actuation force, and is shown to be capable of grasping objects of varying size and shape.

Most linkage-based designs utilize successive four-bar mechanisms which transmit force from an actuator at the base [23, 24]. Elastic elements and mechanical stops are used to restore the system to an open position. A group at École Polytechnique de Montréal has extended the four-bar design to develop a small surgical gripper utilizing only compliant mechanisms [25].

As an extension of the concepts used in the design of the four-bar linkage systems, Almasri and Ouezdou developed an underactuated hand driven by a single motor through the use of gear trains [26]. A group at Clemson University used pneumatics to fill tubes with air, which act as the fingers of the hand [27]. Additionally, collaborative efforts led by Walker of Clemson University have developed numerous iterations of trunk-like mechanisms for compliant grasping and manipulation [28].

Recently, a group at Yale University attached an underactuated hand to the underside of a helicopter [29]. Their work focuses on picking up objects and the effect on flight dynamics, but

landing is still accomplished using traditional landing skids. There has been no investigation of bird-feet-inspired or underactuated graspers for perching.

1.5 Thesis Organization

The goal of this research is to design a passive system that enables rotorcraft to perch on a variety of surfaces. The research focused on the design and analysis of a foot consisting of a compliant gripper and a leg that serves as a passive actuator for the foot. The information is presented as a compilation of two papers. In Chapter 2 is work submitted to the 2011 IEEE/RSJ International Conference on Intelligent Robots and Systems [30], which summarizes the work conducted to complete a first prototype. This chapter focuses on the design and analysis of a cable-driven underactuated gripping foot and a passively-actuating leg designed with a single-material compliant mechanism structure. In Chapter 3 is work submitted to the IEEE/ASME Transactions on Mechatronics focused section on bio-inspired mechatronics [31] detailing the design and testing of a second, improved prototype. This chapter focuses on a design iteration for the actuating leg which offers improved performance by using a four-bar linkage. A detailed analysis of the system is presented and functional testing of the system is completed. Finally, Chapter 4 offers recommendations for further research.

CHAPTER 2

FIRST PROTOTYPE: COMPLAINT LEG AND FOOT MECHANISMS

This chapter consists of work presented at the 2011 IEEE/RSJ International Conference on Intelligent Robots and Systems [30]. This work was done in collaboration with a senior design team in the Department of Mechanical Engineering (Justin Bird, Taylor Isom, Christopher Johnson, Jason Kallman, and Jason Simpson), who were integral in the development of the leg, and Raymond King who aided in the development of the toes during an IGERT lab rotation. My contributions to the work include advising and collaboration in the development of the leg and foot, analysis of the two systems, and documentation of the results.

2.1 Mechanism Design

Our perching mechanism was developed as a compilation of two components: grasping via the foot and actuation via the leg. The foot design is an underactuated tendon-driven structure that requires a single actuating force. This actuation force comes from the leg structure, which converts vertical motion of the rotorcraft into tendon displacement. The two components are integrated, creating a passive landing gear.

2.1.1 Grasping Foot

A desirable characteristic of the bird foot is the underactuated structure. This allows the toes to passively conform to unknown surface shapes. Underactuated graspers have been studied intensely, so we drew inspiration from the large body of work for our initial design. Of particular interest to us is an underactuated design of Dollar and Howe in which an 8-dof four-fingered hand is controlled using a single actuator [22]. Their design uses flexible joints between stiff link segments with a cable to transmit actuation force, and is shown to be capable of grasping objects of varying size and shape.

Our foot is a simplified variation on [22]. Using a waterjet, individual toes were cut from a sheet of polyurethane (McMaster-Carr, Item # 8716K736), using notches to create flexible joints. Hollow tubing was attached to each toe segment for tendon routing. This simple design was chosen for ease of manufacturing and scalability.

Due to the passive actuation method, detailed in the following section, the actuation force is limited by the weight of the rotorcraft. For this reason, friction and joint stiffness are

important in the construction of our toes. Friction forces from the tendon reduce the amount of available gripping force; as such, it is should be minimized. For this prototype, friction reduction was performed qualitatively by experimenting with various tendon and tube materials. The materials selected are 12 lb fishing line (Zebco Omniflex monofiliment) and PTFE tubing (McMaster-Carr, Item # 5239K23). Additionally, locations where the tendon changes direction causes large contact forces, increasing friction. By using curved surfaces to reduce extreme bending, friction is reduced.

In order to study grasping behavior, we developed a model for individual joints and considered kinematic motion of a series of connected toe segments. Each toe joint is characterized by the parameters shown in Fig. 2.1. Furthermore, each joint can be classified as a small-length flexural pivot and is represented by its pseudo-rigid-body model, Fig. 2.2(a), as a pin joint with a torsion spring of stiffness $K = EI/l_0$, where E is the Young's modulus, I is the cross-section moment of inertia, and l_0 is the flexible segment length [32].

Because our flexible segment does not have a uniform cross-section due to the notch angle, validation of the model is necessary. By hanging known weights from samples with varying parameters, we were able to investigate the instantaneous center of rotation (ICR) and stiffness of each joint. Though the ICR location varied significantly between samples, it remained relatively stationary for individual joints (Fig. 2.3), validating the pin-joint approximation. Using the relationship $K = M/\theta$, where M is the moment applied to the joint and θ is the angular deflection of the joint, the stiffness K, which is linearly related to the geometric term wh^3/l, can be experimentally determined (Fig. 2.4).

Combining joints in series produces a toe structure that can passively comply to a surface. Development of our toe is based on two central requirements: 1) for the largest workspace, and thus largest range of gripping capability, it is desirable for the joints to deflect in order from proximal to distal; and 2) each joint should be able to return to minimal deflection with no applied tendon tension.

The first requirement can be satisfied by studying the basic model shown in Fig. 2.2(b). When at static equilibrium, $M_0 = M_1 = M_2 = \ldots = M_n = F_t a$. Also, because each joint

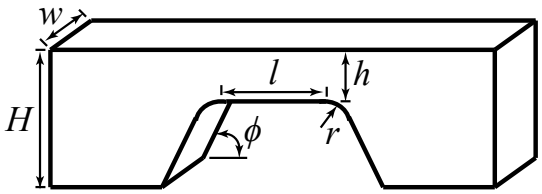

Figure 2.1. Parameters characterizing joint geometry. w is the width of the toe, H is the height of the toe, h is the height of the joint, l is the length of the joint, r is the radius of the joint fillet, and ϕ is the notch angle.

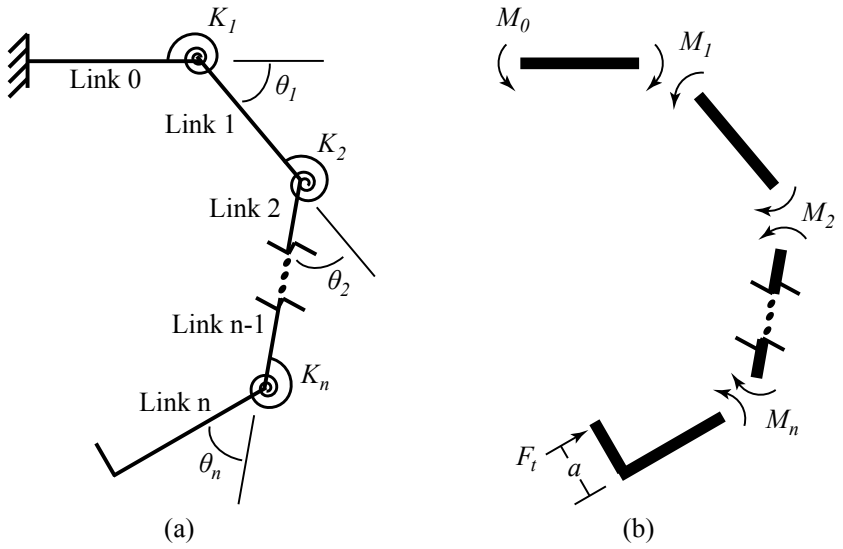

Figure 2.2. Simple model of an n-phalanx toe moving through free space. (a) Pseudo-rigid–body model of toe. K_n is the joint stiffness of the n^{th} link and θ_n is the angular displacement of the n^{th} link. (b) Free body diagram of toe. M_n is the moment of the n^{th} joint, F_t is the tendon tension, and a is the distance from rotation to the tendon attachment.

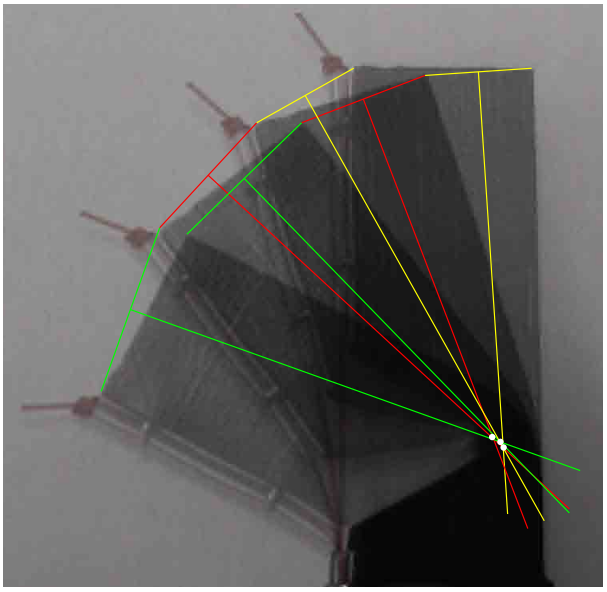

Figure 2.3. Instantaneous center of rotation (ICR) does not vary significantly as a joint deflects. Image overlays joint at four deflection points and the ICR is designated by the white dots, and determined by drawing the perpendicular bisectors of the line segments connecting similar points between deflections.

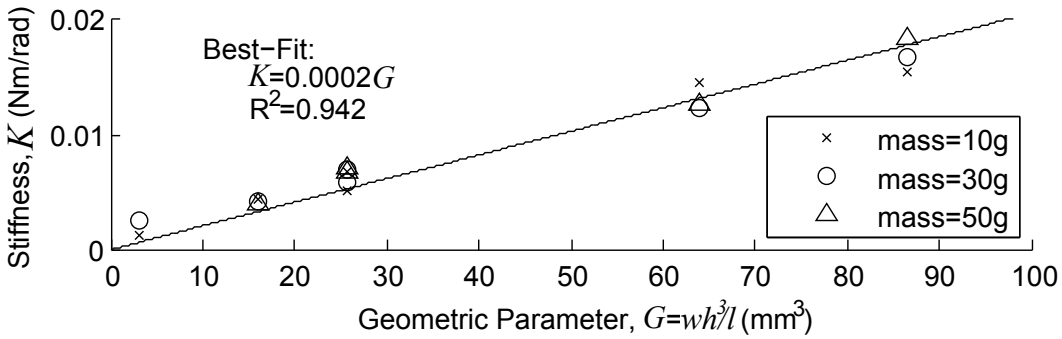

Figure 2.4. Experimental data showing that joint stiffness is linearly related to the geometric term wh^3/l for the joint shown in Fig. 2.1.

is modeled as a pin/torsion spring mechanism, we know that $M_n = K_n\theta_n$, or equivalently, $\theta_n = F_t a/K_n$. It follows that for a given tension, joints with smaller spring constants will experience larger deflections. Thus, enforcing that $K_1 < K_2 < ... < K_n$ satisfies the first requirement. The importance of having a large workspace is demonstrated in Fig. 2.5. Notice how the gripping ability changes for each joint pattern. The top row shows a toe with the proposed pattern, $K_1 < K_2 < K_3$. The toe makes contact with the object starting with the first segment, followed by the second then third, making a successful form closure. The middle row shows a toe with the pattern $K_1 = K_2 = K_3$. For the perch shown, the toe is able to make a form closure but each segment makes contact at roughly the same time. For an unsymmetrical perch this toe will not be able to grip reliably. The bottom row shows a toe with the pattern $K_1 > K_2 > K_3$. This toe experiences significant deflection at the third joint first, which causes the toe to miss closure around the perch.

Figure 2.5. Depiction of how joint stiffness patterns affect form closure. (Top row): $K_1 < K_2 < K_3$; (Middle row): $K_1 = K_2 = K_3$; (Bottom Row): $K_1 > K_2 > K_3$.

To satisfy the second requirement, we enforce $K_1 > K_{1min}$, where K_{1min} is determined by the weight of the distal portion of the toe supported by the first joint. Because the first joint will experience the most weight, and each successive joint is stiffer than the previous, it follows that each joint satisfies the second requirement so long as the first joint does. The above constraints are used to create three identical toes, which are attached to the leg using an adaptation of the anisodactyl arrangement, shown in Fig. 2.6.

2.1.2 Bioinspired Leg Actuator

Underactuated grippers have been extensively studied, but current solutions require actuation via traditional means such as a motor. For a perch-and-stare application, continuously expending power to hold a grip is undesirable. Possible solutions include the use of a nonbackdrivable system or a locking mechanism, however these would still require power to initiate and release the grip. Our design draws inspiration from the unique adaptation developed by song birds that enables passive actuation. This bioinspired design must satisfy two requirements: 1) tendon path length must increase as the mechanism collapses; and 2) rotorcraft center of gravity must move in a predictable manner. The first idea is imperative for passive actuation and the second accounts for system stability during the landing maneuver.

Inspired by the single-material design of the toes, we investigated a concept that has evolved into that shown in Fig. 2.7. This design is mimetic of a bird's leg, consisting of an ankle and knee joint. The structure is formed using a waterjet to cut the shape from a sheet of polycarbonate (Laird Plastics), which makes the prototype easy to manufacture.

In order to satisfy the requirement that the tendon path must increase in length while the leg collapses, knee-cap structures were designed at each joint. By covering a compliant segment with a stiff knee-cap, as the joint deflects the knee-cap creates a varying gap length for the tendon to cover. As the tendon requires more length to cover this gap, it will pull at the foot causing it to close. Additionally, the knee-caps provide a gradual curve for tendon routing, which reduces friction at the points where the tendon changes direction.

The flexible joint was made quite thin in order to reduce the force required to collapse the leg. Any energy utilized in this capacity will reduce the amount of energy available for closing the foot and gripping the perch. The stiffness of each joint can be predicted by studying the

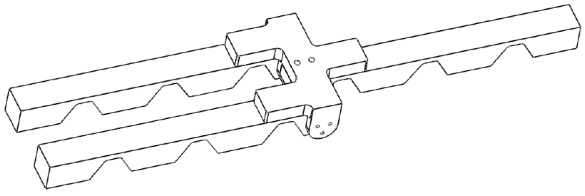

Figure 2.6. SolidWorks model of three-toe foot and mounting device.

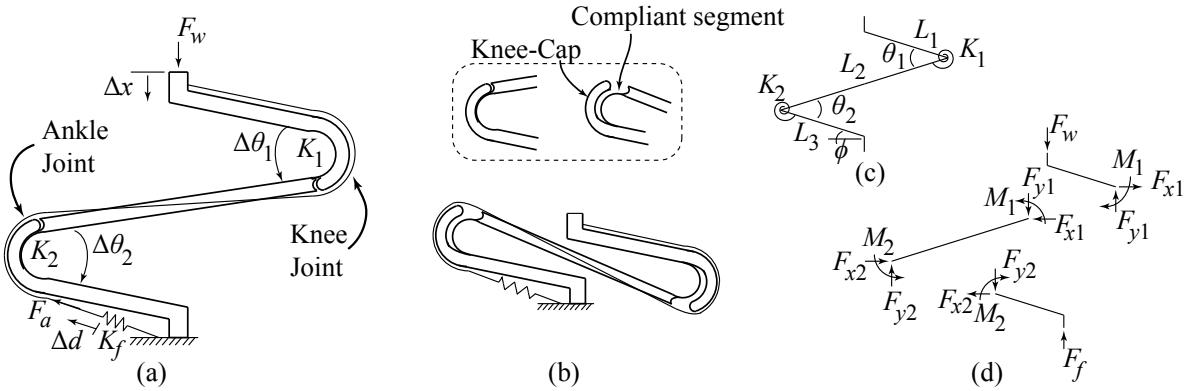

Figure 2.7. Leg mechanism used for passive actuation. (a) Drawing of leg, where F_w is the weight of the rotorcraft, Δx is the vertical displacement of the rotorcraft, $\Delta\theta_n$ is the angular displacement of each leg joint, Δd is the linear displacement of the tendon, F_a is the actuating tension, K_n is the stiffness of each joint, and K_f is the effective spring constant of the foot. (b) Leg in collapsed state. Inset depicts the joint functionality. (c) Pseudo-rigid-body model of leg, where θ_n is the angle between leg segments, L_n is the length of each leg segment, and ϕ is the fixed angle at which the leg leaves the foot. (d) Free body diagram of leg.

pseudo-rigid-body model of an initially curved cantilever beam, as presented in [32]. Similar to experiments with the toe, known forces were applied to knee joints of varying geometries and the stiffness is again found to be linearly related to a geometrical term wh^3/l where the terms w, h, and l are analogous to the parameters depicted in Fig. 2.1.

For a bird to remain stable while standing or perching, its center of gravity is located directly above, and centered between, the feet [14]. Similarly, the rotorcraft center of gravity should rest directly above the foot of the landing gear. Since the landing gear is designed to perch on a variety of geometries, the tendon will displace by varying amounts, causing the body of the rotorcraft to sit at various heights above the perch. For this reason, it is not sufficient to design a mechanism that only centers the position when fully collapsed; the center of gravity must remain vertically aligned with the foot through the entire motion. Furthermore, the collapsing motion should not exert a moment on the foot that would cause it to move out from under the body.

Design for the latter requirement is achieved by studying the leg model, Figs. 2.7(c,d); each rigid segment must be in static equilibrium. Balancing forces in the x and y directions, $F_{x1} = F_{x2} = 0$ and $F_w = F_{y1} = F_{y2} = F_f$. Assuming that the leg remains vertically centered, a moment balance of each link produces

$$L_1 = \frac{M_1}{F_w \cos\frac{\theta_1}{2}}; \quad L_2 = \frac{M_1 + M_2}{F_w \cos\frac{\theta_2}{2}}; \quad L_3 = \frac{M_2}{F_w \cos\frac{\theta_2}{2}}. \tag{2.1}$$

Designing the leg such that $K_1 = K_2$, assuming $\theta_1 = \theta_2$, and noting that $M_1 = M_2 = K_1\theta_1$, (2.1) reduces to constrain the leg links such that

$$L_1 = \frac{1}{2}L_2 = L_3. \tag{2.2}$$

In order to minimize lateral motion of the rotorcraft while perching, a geometric balance is performed. Setting the base of the leg as a zero reference point and using the constraint defined by (2.2), the horizontal location of the top of the leg is calculated as:

$$Y_{leg} = 2L_1 \left(\cos\left(\theta_1 - \phi\right) - \cos\phi\right). \tag{2.3}$$

Minimizing (2.3) over a desirable range of θ_n gives a value of ϕ producing the smallest deviation from vertical.

Our design mimics the functionality of a bird's leg and enables passive actuation of an attached tendon-driven gripper. By following the described constraints, the center of mass of an attached rotorcraft will stay vertically centered over the foot. Attaching two symmetric legs to the underside of a rotorcraft should create a platform for stable perching.

2.1.3 Mechanism Integration

Integrating the foot and leg for successful perching requires a careful consideration of force balance. First, we need to consider the distribution of tendon tension and displacement between the three toes. While unrestricted, each toe should move at the same rate, however if one toe becomes fully constrained by the environment, the remaining toes should be able to continue motion until a complete grip is obtained. Similar to [22] and [19], this is achieved through the design of a differential tendon system, shown in Fig. 2.8. In order to simplify construction, the foot is mounted to the leg such that orientation is opposite of that found in nature; though expected to be minimal, any resulting consequences need to be further examined. The tendon routed from the leg is tied to one side of the pulley mount and the front toe is tied to the opposite side of the mount. The two back toes are connected by a single tendon, routed around the pulley. The tendon in each toe will displace at equivalent rates through open space, providing symmetric closure. If motion in one of the back toes is constrained, the pulley system will allow the remaining toes to move Δd and $2\Delta d$ for the front and back toe, respectively. If

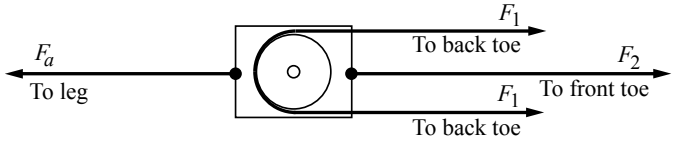

Figure 2.8. Differential system applied to tendons, where F_1 and F_2 are the tendon tensions in individual toes and F_a is the tendon tension applied by the leg. Through open space, each toe moves at equivalent rates. Once one toe is fully constrained by the environment, the remaining toes continue motion until a complete grip is made.

the front toe makes contact before the back toes, motion will continue in all three toes until the landing surface is centered appropriately in the foot.

Furthermore, through open space, this setup creates an equal force distribution among each of the toes, such that $F_1 \approx F_2 \approx F_a/3$. This is an approximate relationship because the tendon does not necessarily depart the pulley in a direction parallel to F_a; deviation will cause slight variations in tension. Once motion in one back toe is constrained, the two back toes will still experience equivalent tension, but the tension in the tendon of the back toes will increase at twice the rate of the front toe due to the different rates of motion.

Another important design requirement is that the foot be able to close fully given the available force. The relationship between tension and rotorcraft weight is determined by an energy balance of the system depicted in Fig. 2.7(a):

$$F_w \Delta x = \frac{1}{2} K_1 \Delta\theta_1^2 + \frac{1}{2} K_2 \Delta\theta_2^2 + \frac{1}{2} K_f \Delta d^2. \tag{2.4}$$

By substituting the relationship $F_a = K_f \Delta d$ and assuming $K_1 = K_2 = K$ and $\Delta\theta_1 = \Delta\theta_2 = \Delta\theta/2$, rearranging (3.17) gives the relationship between the applied tension and the weight of the rotorcraft:

$$F_a = \frac{2F_w \Delta x - K\Delta\theta^2/2}{\Delta d}. \tag{2.5}$$

Geometrical relationships exist between Δx, $\Delta\theta$, and Δd, which can be utilized to further characterize the tendon tension. The relationship between Δx and $\Delta\theta$ is determined by assuming that the body stays vertically aligned with the foot. This assumption is justified by using the described design process, which causes the body to follow a nearly straight line. In reality, the alignment deviates slightly from vertical and this assumption underestimates the change in angle for a given vertical displacement. Studying Fig. 2.9(a), the Law of Cosines can be used to show that

$$\Delta\theta \approx 4 \sin^{-1}\left(\frac{\Delta x}{4L}\right). \tag{2.6}$$

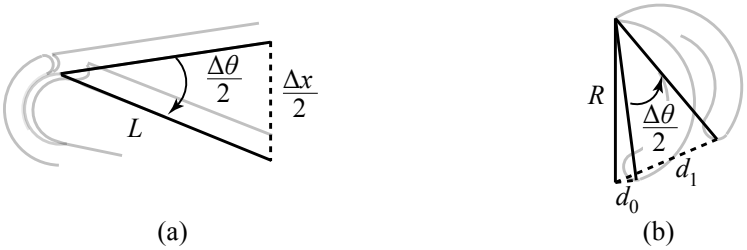

Figure 2.9. Geometrical constraints of the actuating system. (a) Geometrical relationship between Δx and $\Delta\theta$, where L is the link length (L_1) and $\Delta\theta$, Δx are as defined previously. (b) Geometrical relationship between $\Delta\theta$ and Δd, where R is the outer knee-cap radius, d_i is the tendon path length and $\Delta\theta$ is as defined previously.

The relationship between $\Delta\theta$ and Δd is determined by studying Fig. 2.9(b). Here, $\Delta d/2 = d_1 - d_0$. By making a simplifying assumption that $d_0 = 0$, we can use the Law of Cosines to show that

$$\Delta d \approx 4R \sin\left(\frac{\Delta\theta}{4}\right) = \frac{R\Delta x}{L}. \tag{2.7}$$

For our system, this assumption introduces less than 10% error, but does overestimate the amount of tendon displacement for a given change in joint angle. This equation also provides a design metric, as a certain radius is required to achieve a desired amount of tendon travel.

Substituting (2.6) and (2.7) into (2.5) produces an equation that relates the amount of total tension available for actuating the foot and grasping, based on the weight and vertical displacement of the rotorcraft:

$$F_a = \frac{2L}{R}\left(F_w - \frac{2K\left(\sin^{-1}\left(\frac{\Delta x}{4L}\right)\right)^2}{\Delta x}\right). \tag{2.8}$$

Due to the simplifying assumptions made in the development of this equation, if K is sufficiently small, this is actually a conservative estimation of the tension, which helps offset nonconservative modeling assumptions (e.g., no friction in tendon routing). The force available for grasping can be determined by subtracting the tension required to overcome toe stiffness in a given configuration from (2.8).

2.2 Results and Discussion

A prototype was constructed using the methods described, and is shown in a relaxed state in the left column of Fig. 2.10. In order to increase the amount of friction at the grip, a soft Buna-N foam (McMaster-Carr, Item # 93745K21) was attached to the surface of each toe segment. The final prototype weights 96 g. This prototype was tested on two cylindrical rods with diameters of 49 mm and 33 mm by hanging two 100 g weights on the leg, which was chosen as a convenient weight and is not meant to be representative of rotorcraft weight. Successful perching is demonstrated in the center and right columns of Fig. 2.10.

Our prototype shows that passive perching on curved surfaces can be achieved using an avian-inspired approach. However, this design is an un-optimized solution, and improvements are currently being investigated. First, although the compliant leg mechanism is desirable for manufacturablity and scalability, at this scale the tension forces are too large and the compliant members in the knee and ankle begin to deflect at undesirable locations. This causes a decrease in performance, as extra energy in the system acts to deform these members rather than increase tension. The deformation creates significant stresses, which cause the compliant members to fatigue prematurely. The choice of polycarbonate for the flexure also contributes to fatigue problems. Second, the lateral stability of the leg is weak due to the long, thin members, which will reduce stability in the whole system under reasonable disturbances.

Figure 2.10. Demonstration of functional prototype. (Left column): Image of landing gear in its relaxed state. (Center column): Series of images showing a successful perch on a rod of diameter of 49 mm. (Right column): Series of images showing a successful perch on a rod of diameter of 33 mm.

Currently, in order to work around these difficulties, the toes are designed such that a complete grip is possible at very low tension, so that the leg joints do not deform significantly. This design consideration directly corresponds to weak compliant members at each toe joint, which means the toes sag under their own weight when the system is relaxed. Methods currently under consideration to reduce sag include adding a pre-curve to the toe (similar to the blades of a helicopter or wings of a plane) and selecting lighter-weight materials. Additionally, a grip-force analysis is being conducted so that we can predict the ability of the system to resist environmental disturbances while perched.

2.3 Conclusions

This first prototype demonstrates the concept of a passive, avian-inspired perching mechanism. Successful perches were made and were stable under small disturbances. Our results show promise that future iterations should perform well as a solution for passive, compliant landing gear for perch-and-stare applications on curved surfaces.

CHAPTER 3

SECOND PROTOTYPE: QUADROTOR PERCHING WITH AN IMPROVED MECHANISM

This chapter consists of work submitted to the IEEE/ASME Transactions on Mechatronics focused section on bio-inspired mechatronics [31]. It presents an improved design and subsequent stability evaluation. The work was done in collaboration with a senior design team in the Department of Mechanical Engineering (Justin Bird, Taylor Isom, Christopher Johnson, Jason Kallman, and Jason Simpson), who were integral in the development of the leg. My contributions to the work include advising and collaboration in the development of the leg and foot, analysis of the two systems, design and implementation of stability tests, and documentation of the results. An image of the completed system is shown in Fig. 3.1. SolidWorks models of the design can be found the Appendix.

Figure 3.1. Quadrotor perching on a cylindrical railing. The landing gear is actuated by the weight of the quadrotor and creates a grip strong enough to withstand small-to-moderate environmental disturbances.

3.1 Passively Actuated Leg

This section presents a design iteration for the leg mechanism that improves upon our previous work by increasing stability and cyclic life. The most important function of the leg is its ability to convert vertical motion into tendon actuation, which depends on the geometry of the leg segments. Similar to the previous design, the leg consists of a knee and ankle joint and three rigid segments: the thigh, shin, and heel. The key difference is that the single-material compliant joints have been replaced with pin joints; this reduces fatigue, reduces out-of-plane motion, generates more idealized behavior, and allows for a more exact analysis of the system.

Repeated here for clarity, the bioinspired design must satisfy two requirements: 1) tendon path length must increase as the mechanism collapses; and 2) aircraft center of gravity must move in a predictable manner. The first idea is imperative for passive actuation and the second accounts for system stability during the landing maneuver.

The first requirement is satisfied by using round cams at each joint, which cause the tendon to wrap around a larger portion of the circumference as the leg collapses. The second requirement is satisfied by enforcing that the shin is twice the length of the thigh and heel, as discussed in Chapter 2. Additionally, a parallelogram linkage for the shin, with pin joints vertically aligned, enforces that the two joints deflect at the same rate and that the aircraft body keeps a constant orientation.

We first present the design for keeping center of mass over the foot. Second, we present how the vertical motion of the leg relates to a change in tendon path length, which is necessary to actuate the attached gripping foot. Finally, we present how the weight of the aircraft relates to the amount of tension available in the system, which corresponds to the grip strength of the foot.

3.1.1 Centering Rotorcraft Mass

As the rotorcraft lowers onto the perch, its center of mass must stay centered over the foot and the leg should not exert a moment at the foot that causes it to move out from under the body. Studying the free body diagram presented in Fig. 3.2 provides design rules that must be followed to enforce proper motion. First, summing forces in the y-direction, and assuming the vertically aligned pin joints support equal forces:

$$F_w = \frac{1}{2}F_{y1a} = \frac{1}{2}F_{y1b} = \frac{1}{2}F_{y2a} = \frac{1}{2}F_{y2b} = F_p. \tag{3.1}$$

Second, summing forces in the x-direction:

$$F_{x1a} = F_{x1b} = F_{x2a} = F_{x1b}. \tag{3.2}$$

Finally, performing a moment balance on links 1 and 3 and solving for L_1 and L_3:

$$L_1 = \frac{F_{x1a}p}{F_w \cos\phi}; \quad L_3 = \frac{F_{x2b}p}{F_p \cos\phi}. \tag{3.3}$$

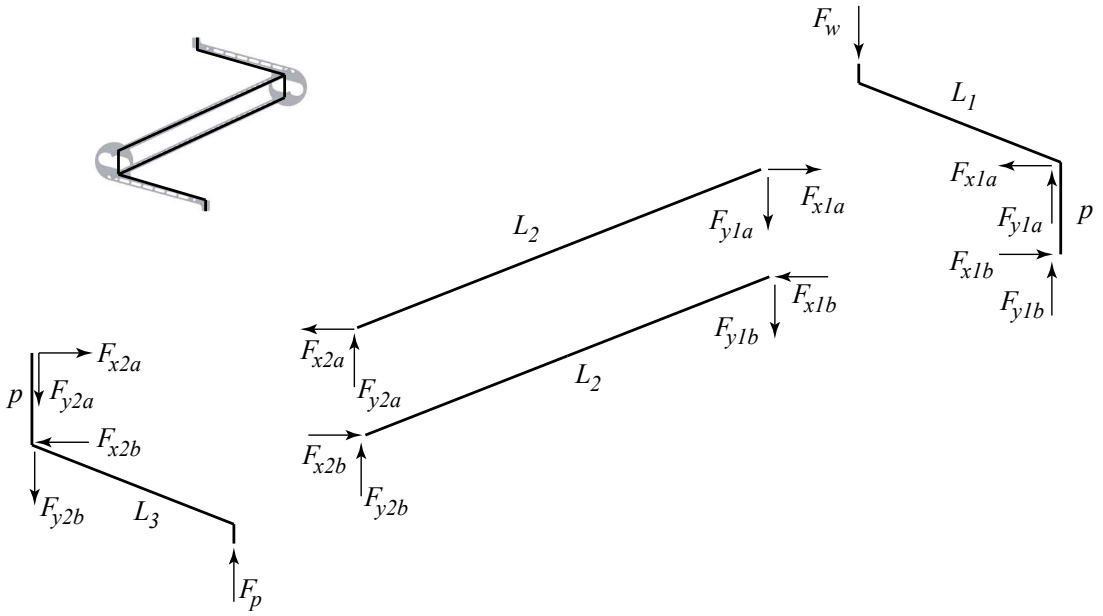

Figure 3.2. Free body diagram of leg. F_w is the force due to the weight of the rotorcraft, F_p is the force applied by the perch, and the remaining force represent reactive forces between links. Inset depicts full leg with link segments indicated.

Substituting the force balances (3.1) and (3.2) results in the design requirement, $L_1 = L_3 = L$. The force/moment balance does not place requirements on L_2, but in order to keep the rotorcraft COM over the foot, $L_2 = 2L$. A different value for L_2 could be used if the leg is not attached directly below the rotorcraft's COM, however this would impose a moment at the top of the leg, which would alter the moment balance of the system and change the requirements on L_1 and L_3.

The position of the aircraft mounting point, relative to the foot, is dependent on the angular deflection of each joint, Fig. 3.3. Placing the origin, $\boldsymbol{O}$, at the foot, the location of each joint and the aircraft body are determined as follows:

$$\begin{aligned} A &= (A_x, A_y) = \left(-L\cos\phi, L\sin\phi + \frac{p}{2}\right) \\ B &= (B_x, B_y) = (A_x + 2L\cos\alpha, A_y + 2L\sin\alpha) \\ C &= (C_x, C_y) = \left(B_x - L\cos\phi, B_y + L\sin\phi + \frac{p}{2}\right) \end{aligned} \tag{3.4}$$

where $\alpha = \theta - \phi$.

It is desirable to minimize the horizontal motion of the aircraft during collapse; this can be done by running a minimax optimization on $|C_x|$ of (3.4) with respect to ϕ over a desirable range of motion for each joint, θ. For the range $0 \leq \theta \leq 40$ degrees, the optimal value of ϕ is 16.5 degrees. Fig. 3.4(a) shows the horizontal deviation for $\phi = 16.5$ degrees, $L = 152.4$ mm and $p = 38.1$ mm; the values of L and p are the dimensions used in our prototype, which were

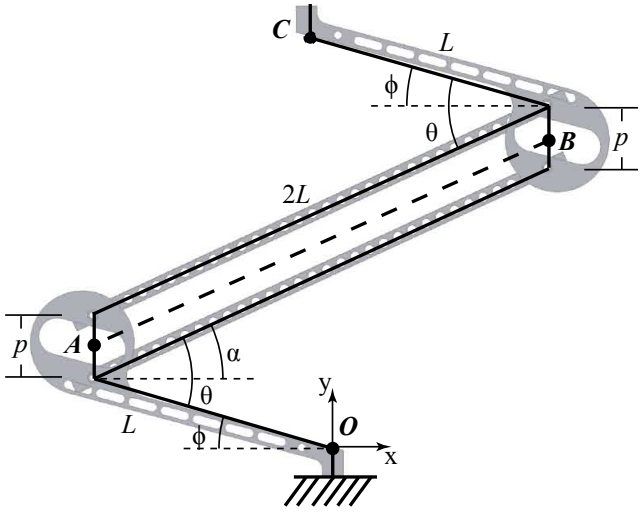

Figure 3.3. Geometric model of leg superimposed on a SolidWorks rendering. L is the length of the thigh and heel links, p is the distance between the joints of the parallel shin links, θ is the angle between links, α is the angle between the shin and horizontal, and ϕ is the fixed angle between the heel/thigh and horizontal. $\boldsymbol{O}$ is the origin where the foot attaches to the leg, $\boldsymbol{A}$ is the first pivot point, $\boldsymbol{B}$ is the second pivot point, and $\boldsymbol{C}$ is the point at which the aircraft attaches to the leg. $\boldsymbol{A}$ and $\boldsymbol{B}$ are located half way between the physical pin joints of the shin links. The exact locations of $\boldsymbol{O}$ and $\boldsymbol{C}$ are arbitrary, but once selected all other parameters are referenced from their location.

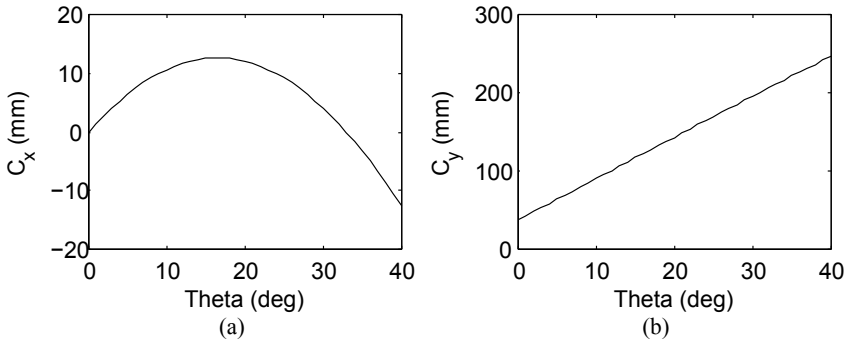

Figure 3.4. Plot of aircraft motion based on angle of joints. $\phi = 16.5°$, $L = 152.4\,\text{mm}$, and $p = 38.1\,\text{mm}$ (a) Horizontal deviation from vertical. (b) Vertical height of aircraft above foot.

arbitrarily chosen to create a mechanism roughly scaled for a quadrotor, achieving at least the minimal force required to actuate the foot. Similarly, the vertical motion of the aircraft is shown in Fig. 3.4(b).

3.1.2 Vertical Motion to Tendon Pull

The tendon routing through the leg is depicted in Fig. 3.5. The change in tendon path length is dependent on two factors: a wrapping of the tendon around each cam, and a change in length of the tangent path between the two cams. By designing the two cams to be symmetric, the

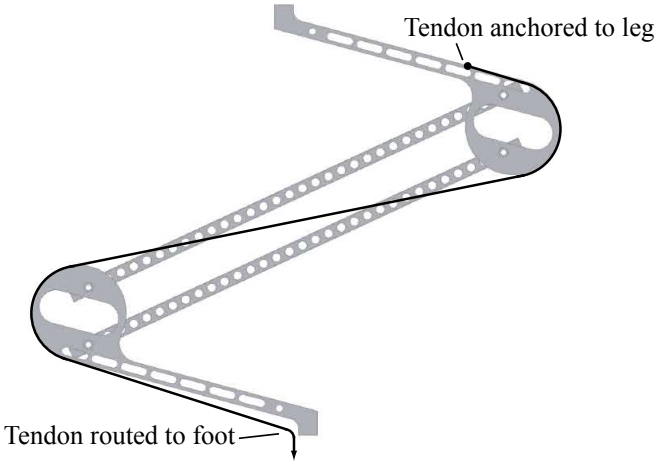

Figure 3.5. Tendon routing. The tendon is anchored to the leg at the thigh just before the circular cam. The tendon then wraps around cams such that it runs along an inner tangent line between the two cams. Finally, the tendon is routed towards the foot using a pulley system discussed in the previous chapter.

model reduces to two sets of identical triangles that intersect at a common point, as seen in Fig. 3.6(a). Studying a single set of triangles, Fig. 3.6(b), the tendon path length (3.5) is determined by summing the arc length of the tendon in contact with the cam (3.6) and the length of the tangent line between the two cams (3.7). t_{arc} is defined by assuming that the tendon wraps 3/4 of the circular cam when $\gamma = 0$ degrees; although the tendon will actually contact slightly less than 3/4 of the circumference, we are concerned with the change in path length, not the actual path length, so this simplifying approximation does not affect the final result.

$$t = t_{arc} + t_{tan} \tag{3.5}$$

$$t_{arc} = 2r\left(\frac{3\pi}{2} - \gamma\right) \tag{3.6}$$

$$t_{tan} = T \tag{3.7}$$

The task now lies in determining values for γ and T. Examining Triangle 1, trigonometric identities can be used to first determine the dimension c and then the angle γ_1:

$$\left(\frac{c}{2}\right)^2 = q^2 + L^2 - 2qL\cos(\pi - \alpha) \tag{3.8}$$

$$\frac{\sin\gamma_1}{L} = \frac{\sin(\pi - \alpha)}{c/2}. \tag{3.9}$$

Next, examining Triangle 2, geometric and trigonometric identities can be used to determine the dimension T and angle γ_2:

$$r^2 + \left(\frac{T}{2}\right)^2 = \left(\frac{c}{2}\right)^2 \tag{3.10}$$

$$\tan\gamma_2 = \frac{T/2}{r}. \tag{3.11}$$

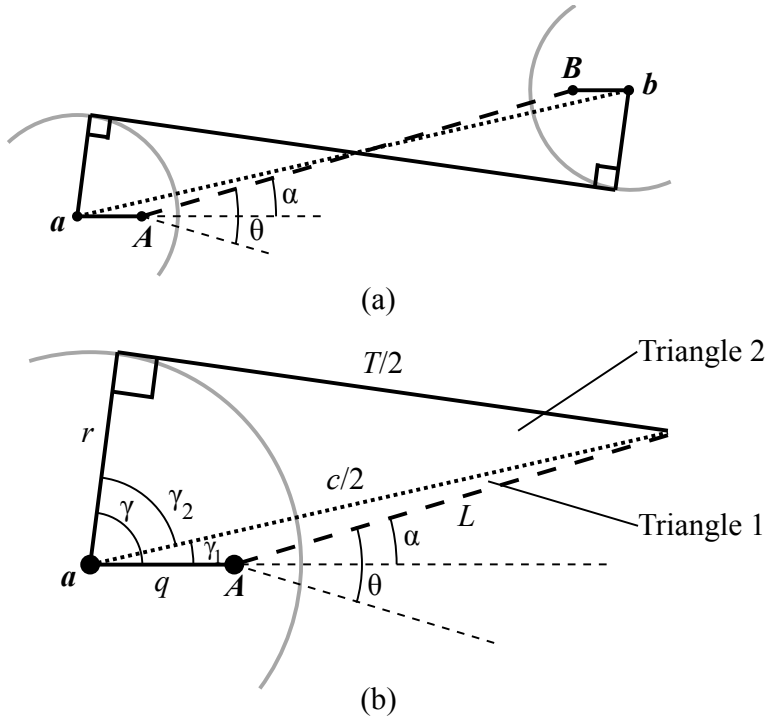

Figure 3.6. Geometry of tendon path length. (a) Total length from joint to joint. (b) Detail view of half the system. θ, α, L, $\boldsymbol{A}$, and $\boldsymbol{B}$ are as defined previously. $\boldsymbol{a}$ and $\boldsymbol{b}$ are the centers of the circular cams, c is the distance between the center of the cams, T is the distance between the tangent points at which the tendon leaves each cam, r is the radius of each cam, q is the distance between the rotation point and the center of each cam (assumed to be horizontal), and γ, γ_1, and γ_2 are defined as shown.

Finally, the angle γ is known, as the sum of γ_1 and γ_2. The two parameters of interest are thus:

$$T = 2\sqrt{q^2 + L^2 - r^2 + 2qL\cos(\theta - \phi)} \tag{3.12}$$

$$\gamma = \tan^{-1}\left(\frac{T}{2r}\right) + \sin^{-1}\left(\frac{L\sin(\theta - \phi)}{\sqrt{q^2 + L^2 + 2qL\cos(\theta - \phi)}}\right). \tag{3.13}$$

A plot showing how the tendon path length changes with vertical motion is presented in Fig. 3.7, where the values of ϕ, L, and p are chosen as before and r is the value used in our prototype, which was chosen to provide an appropriate amount of tendon travel based on our prototype foot. Plots for both $q = 6.35\,\text{mm}$, which is the value on our prototype, and $q = 0\,\text{mm}$ are shown. Subsequent work becomes difficult with $q \neq 0$ due to noninvertible functions, so $q = 0$ is used to further analyze the system; the error introduced in Δt is minimal ($< 3\%$), as demonstrated by Fig. 3.7. Future prototypes should be constructed such that $q = 0$, so that accurate analysis can be performed on the system. Simplified equations for T and γ, with $q = 0$, are subsequently:

$$T = 2\sqrt{L^2 - r^2} \tag{3.14}$$

$$\gamma = \tan^{-1}\left(\frac{T}{2r}\right) + \theta - \phi, \tag{3.15}$$

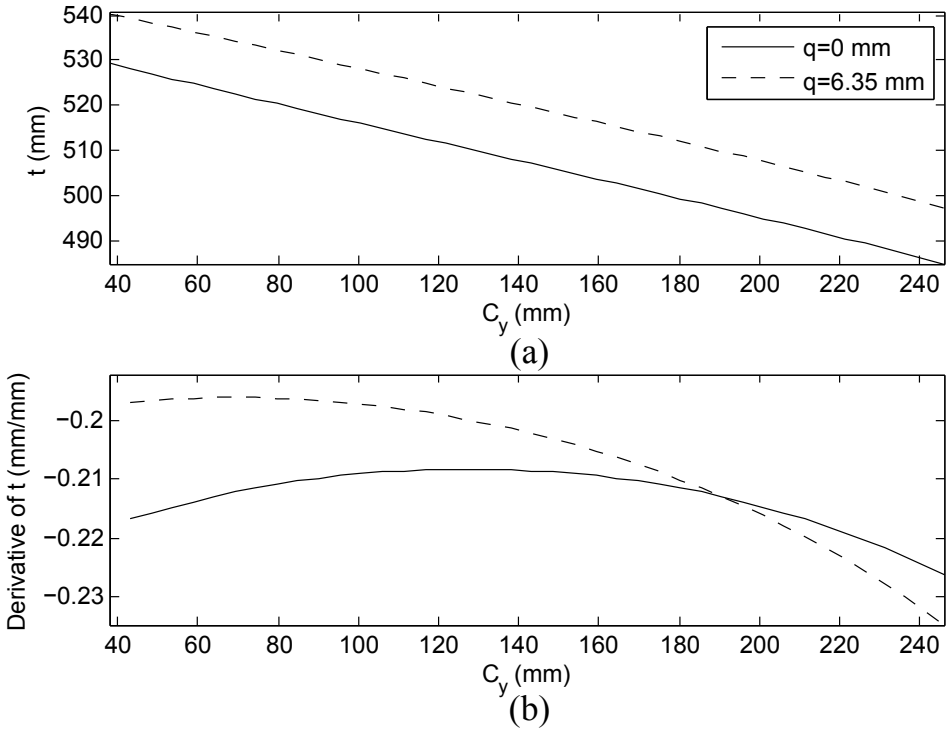

Figure 3.7. Tendon path length vs. vertical displacement. (a) As the leg collapses, the tendon path length increases. (b) Derivative of tendon path length with respect to vertical displacement. The total affect due to q is insignificant ($< 3\%$) for $\phi = 16.5°$, $L = 152.4\,\text{mm}$, $p = 38.1\,\text{mm}$, and $r = 31.7\,\text{mm}$

giving

$$t = 2r\left(\frac{3\pi}{2} - \tan^{-1}\left(\frac{\sqrt{L^2 - r^2}}{r}\right) + \theta - \phi\right) + 2\sqrt{L^2 - r^2}. \tag{3.16}$$

3.1.3 Rotorcraft Weight to Tendon Tension

The amount of tension that a rotorcraft can supply to close the gripper is directly related to the weight of the rotorcraft, F_w. Performing an energy balance on the system shown in Fig. 3.8,

$$F_w\Delta = \frac{1}{2}K_f\delta^2. \tag{3.17}$$

Considering the leg collapsed by some nominal value Δ, collapsing the system by a differential change, $d\Delta$, produces:

$$F_w(\Delta + d\Delta) = \frac{1}{2}K_f\left(\delta^2 + 2\delta d\delta + d\delta^2\right). \tag{3.18}$$

Substituting in (3.17), recognizing that $d\delta^2$ can be neglected, and substituting in the locally linear relationship $F_a = K_f\delta$, (3.18) can be solved for the mechanical advantage of the system,

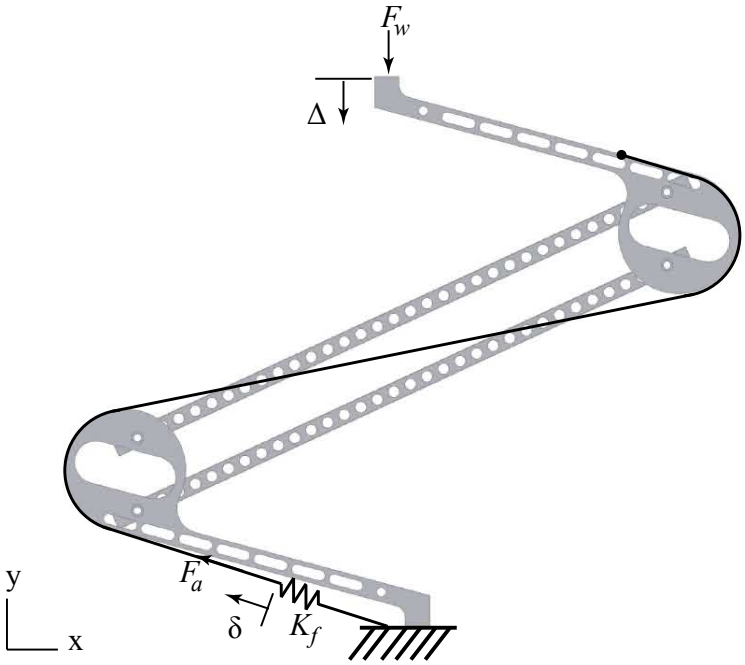

Figure 3.8. Leg model depiction energy balance. F_w is the weight of the rotorcraft, F_a is the tension applied to the foot, Δy is the change in height of the rotorcraft, Δd is the change in tendon path length, and K_f is the effective spring constant of the foot.

F_a/F_w, which relates the weight of the rotorcraft to tendon tension at the foot. Note that $dC_y = -d\Delta$ and $dt = d\delta$, so:

$$\frac{F_a}{F_w} = \frac{d\Delta}{d\delta} = -\frac{dC_y}{dt}. \tag{3.19}$$

Thus, the mechanical advantage of the system is found by differentiating C_y with respect to t.

C_y of (3.4) can be expanded as:

$$C_y(\theta) = 2L\sin(\theta - \phi) + 2L\sin\phi + p. \tag{3.20}$$

But, we need $C_y(t)$, not $C_y(\theta)$, so solving (3.16) for θ gives:

$$\theta = \frac{3\pi}{2} + Q - \tan^{-1} Q + \phi - \frac{t}{2r} \tag{3.21}$$

where $Q = \sqrt{L^2 - r^2}/r$. Thus, substituting (3.21) into (3.20):

$$C_y(t) = 2L\sin\left(\frac{3\pi}{2} + Q - \tan^{-1} Q - \frac{t}{2r}\right) + 2L\sin\phi + p \tag{3.22}$$

Differentiating (3.22) with respect to t produces:

$$\frac{dC_y}{dt} = -\frac{L}{r}\cos\left(\frac{3\pi}{2} + Q - \tan^{-1} Q - \frac{t}{2r}\right). \tag{3.23}$$

The mechanical advantage of the system can be visualized in Fig. 3.9. As the leg collapses, the mechanical advantage increases, reaches a maximum, then begins to decrease; mechanical advantage is between 4.4 and 4.8 through the entire motion.

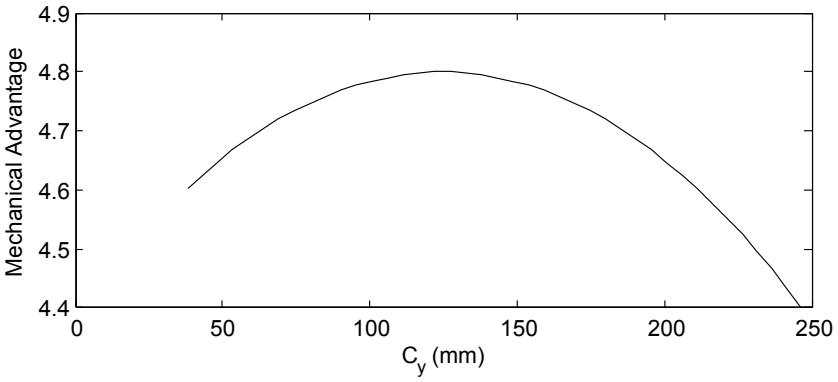

Figure 3.9. Mechanical advantage of leg throughout collapse. As the leg collapses, the mechanical advantage increases, reaches a maximum, then begins to decrease; mechanical advantage is between 4.4 and 4.8 through the entire motion. $\phi = 16.5°$, $L = 152.4\,\text{mm}$, $p = 38.1\,\text{mm}$, $q = 0.0\,\text{mm}$, and $r = 31.7\,\text{mm}$.

3.2 Compliant Gripping Foot

Minimal changes were made to the foot between prototypes. For design detail, refer to Chapter 2. Improved toe models and analysis of the gripping capability are presented in this chapter.

For an underactuated gripper to be effective as a perching mechanism, it must be able to produce a gripping force that can withstand environmental perturbations. Previous work has focused on gripping analysis of underactuated fingers [33], however this work is based on the assumption that a direct actuation torque is applied to the first joint of the finger. In our system, the actuation of each joint is indirect, due to the imposed moment of the tendon tension acting on the distal end of the toe. Because of this indirect actuation, the models presented in [33] cannot be easily adapted to our system. Instead, we propose analysis of the model shown in Fig. 3.10, with which we can compute contact forces between the individual toe links and the perch for a given toe configuration. The model can also be used to predict a toe configuration based on a set of contact forces and tendon tension. For example, motion through free space can be predicted by setting each contact force to zero.

Starting at the most distal, n^{th} link, we can work recursively through the system to find the contact forces on any intermediate link. With this analysis, we are neglecting the friction due to tendon movement, assuming only tension components in the y-direction act on the intermediate links, and assuming that the contact force is applied normal to the midpoint of each link. Furthermore, it can be shown that $\alpha_i = \pi/2 - \theta_i/2$ and $\beta_i = \pi/2 - \theta_{i+1}/2$. Finally, for each joint, $M_i = K_i\theta_i$. A recursive formula for the forces on each link is thus provided by:

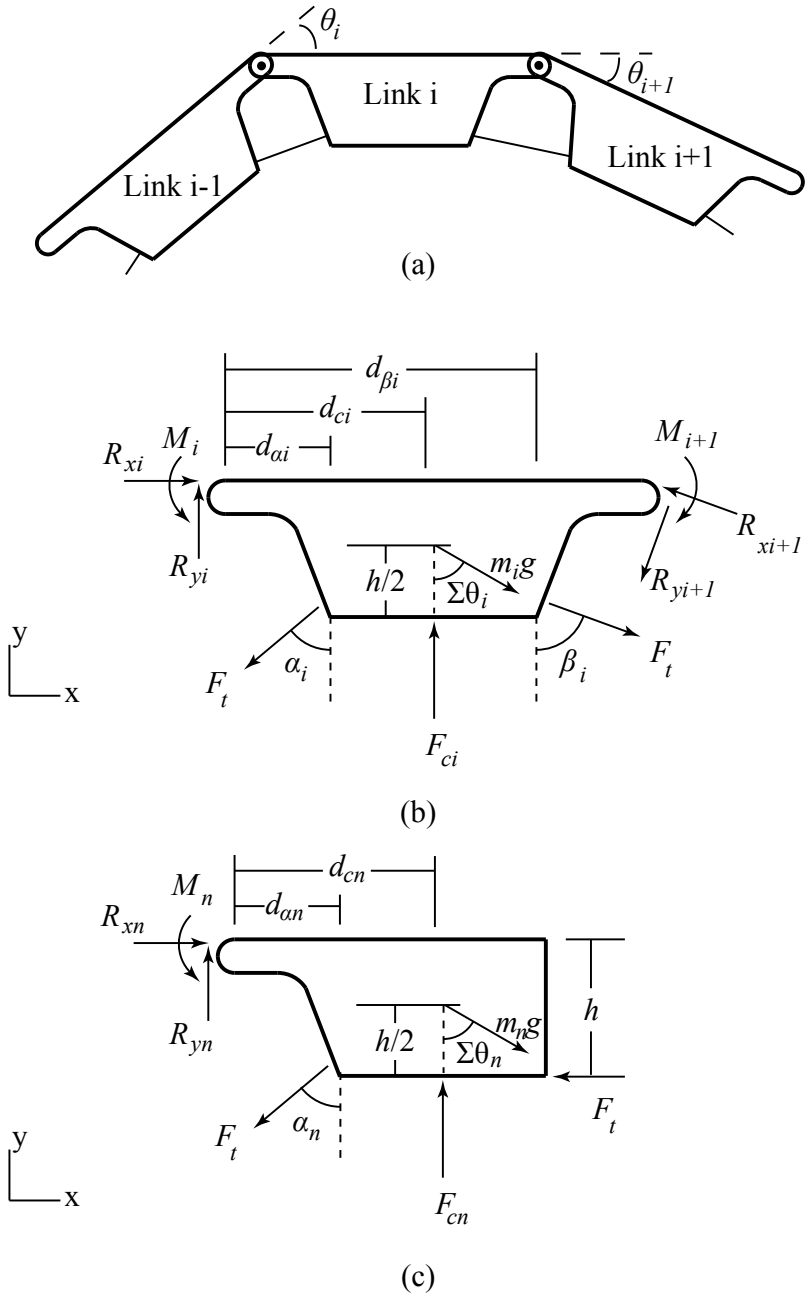

Figure 3.10. Static model of an n-link toe with environmental contact. (a) Parameter and geometric labeling of toe. θ_i is the angular displacement of link i with respect to link $i-1$. (b) Free body diagram of link i. M_i is the moment of joint i, m_i is the mass of link i, g is the gravitational constant, $\Sigma\theta_i$ is the sum of all joint angles from θ_1 to θ_i, F_t is the tendon tension, F_{ci} is the contact force on link i and d_c is the moment arm through which that force is applied, which corresponds to half the link length, α_i and β_i are the tendon departure angles from link i, and d_α and d_β are the moment arms through which the tendon forces are applied. (c) Free body diagram of link n, which is the most distal. h is the moment arm through which the tendon is attached and the remaining parameters are as defined before.

$$F_{cn} = \frac{1}{d_c}\left(F_t\left(d_\alpha \sin\left(\frac{\theta_n}{2}\right)+h\right) - K_n\theta_n + m_n g\left(d_{cn}\cos\Sigma\theta_n - \frac{h}{2}\sin\Sigma\theta_n\right)\right) \quad (3.24)$$

$$R_{xn} = F_t - m_n g \sin\Sigma\theta_n \quad (3.25)$$

$$R_{yn} = F_t \sin\left(\frac{\theta_n}{2}\right) + m_n g\cos\Sigma\theta_n - F_{cn} \quad (3.26)$$

$$F_{ci} = \frac{1}{d_c}\left(F_t\left(d_{\alpha i}\sin\left(\frac{\theta_i}{2}\right)+d_{\beta i}\sin\left(\frac{\theta_{i+1}}{2}\right)\right) + K_{i+1}\theta_{i+1} - K_i\theta_i + 2d_{ci}\left(R_{yi+1}\cos\theta_{i+1} - R_{xi+1}\sin\theta_{i+1}\right) + m_i g\left(d_{ci}\cos\Sigma\theta_i - \frac{h}{2}\sin\Sigma\theta_i\right)\right) \quad (3.27)$$

$$R_{xi} = R_{xi+1}\cos\theta_{i+1} + R_{yi+1}\sin\theta_{i+1} - m_i g\sin\Sigma\theta_i \quad (3.28)$$

$$R_{yi} = F_t\left(\sin\left(\frac{\theta_i}{2}\right)+\sin\left(\frac{\theta_{i+1}}{2}\right)\right) + R_{yi+1}\cos\theta_{i+1} - R_{xi+1}\sin\theta_{i+1} + m_i g\cos\Sigma\theta_i - F_{ci}. \quad (3.29)$$

After adopting this model, it became apparent that the joint stiffness cannot be assumed constant through the full range of deflection as previously stated. In order to accurately determine the stiffness of each joint, a single toe was mounted such that the first link was horizontal and the distal links sagged under their own weight. Calibrated weights were hung from the tendon, using a pulley to convert vertical motion of the weight into horizontal tendon pull, and the deflection of each joint was recorded by studying images taken for each applied weight. The process was repeated three times to analyze repeatability. The deflection results are summarized in Table 3.1 and the subsequent joint stiffness can be visualized in Fig. 3.11. Notice that the joints become stiffer as they deflect through larger angles. This trend was not discovered in the previous model of Section 2.1.1 due to the incorrect assumption that the bending moments at each of the toe joints are identical; the model presented in this chapter demonstrates that for our tendon system, there are additional forces producing moments at the joints other than those due to the most distal connection point.

Table 3.1. Toe joint deflection for applied tension, given in terms of calibrated mass. †Joint notch geometry restricts further motion, stiffness values for deflection not calculated.

	θ_1 Mean ± StDev	θ_2 Mean ± StDev	θ_3 Mean ± StDev
0 g	$41.0 \pm 0.0°$	$14.3 \pm 0.5°$	$7.3 \pm 1.2°$
10 g	$45.7 \pm 0.5°$	$17.0 \pm 0.8°$	$10.3 \pm 0.9°$
20 g	$48.7 \pm 0.5°$	$20.0 \pm 0.8°$	$13.7 \pm 0.5°$
50 g	$60.3 \pm 0.9°$	$31.0 \pm 0.0°$	$25.0 \pm 0.8°$
70 g	$69.7 \pm 1.7°$	$39.0 \pm 1.4°$	$33.0 \pm 1.6°$
100 g	$77.0 \pm 0.0°$†	$51.0 \pm 0.8°$	$43.7 \pm 1.2°$
120 g	$77.0 \pm 0.0°$†	$59.7 \pm 0.9°$	$52.0 \pm 0.8°$
150 g	$77.0 \pm 0.0°$†	$71.7 \pm 0.9°$	$62.7 \pm 1.7°$
170 g	$77.0 \pm 0.0°$†	$79.3 \pm 0.9°$†	$72.0 \pm 0.8°$

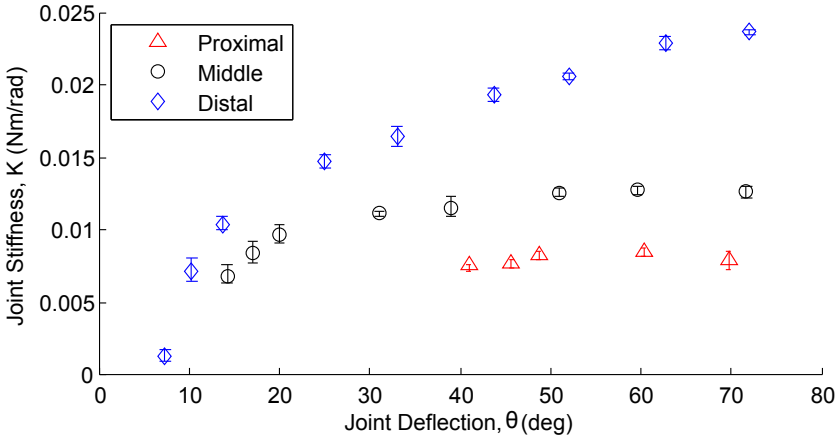

Figure 3.11. Joint stiffness as a function of deflection. Values are calculated using the mean joint deflections reported in Table 3.1. Error bars show the range of K values possible with all permutations of $\pm\sigma$ in joint deflection. Stiffness is nonlinearly related to deflection and increases as the toe deflects further.

The ability of the system to reject disturbances directly corresponds to the grip strength of the foot. The maximum moment disturbance that can be rejected is related to the term $\mu_s r_p \sum F_{ci}$, where μ_s is the static coefficient of friction between the toes and perch and r_p is the approximate radius of the perch. The moment disturbance can be due to any force acting through a distance from the center of the perch; for example, the rotorcraft perching at some angle away from vertical, or a wind gust pushing on the rotorcraft body. From the model, one can expect the contact forces, and thus grip strength, to increase as tendon tension increases; application of the model to a perching rotorcraft is discussed in the next section.

3.3 System Integration

For maximum grasping compliance, it is desirable that each toe be able to move semi-independently. As described in Chapter 2, a pulley block is utilized to allow for differential actuation of each toe. In our previous prototype, monofilament fishing line was used as the tendon material. Although the strength of the line was sufficient to support the applied tension without breaking, it stretched significantly and experienced plastic deformation. Thus, the system did not exert a strong grasp, as tension beyond that required to close the foot acted to stretch the line rather than just tighten the grip. For this new design, the tendon material was upgraded to a fused superline (10lb Berkley FireLine Fused Crystal), which has minimal stretch. Furthermore, in addition to the soft Buna-N foam attached to the surface of each toe segment, coarse sandpaper (60 grit aluminum oxide on cloth backing) was applied to provide greater friction at the grip. Additionally, two mechanical pin-type stops were added to each cam in order to restrain the motion of the leg when freely dangling beneath the rotorcraft. Rather than using a dedicated component to achieve this, the dimension p between the two

shin links can be adjusted in future iterations so that the links stop on each other at a desired angle. Adjusting p will also change how low the aircraft can sit above a perch, as the current shin configuration hits the quadrotor base before a complete grasp is made on small perches.

Two leg/foot mechanisms were attached to a Gaui 330X Quad Flyer. This quadrotor model was chosen because it is affordable and has a frame designed for component additions, which made it particularly easy to attach our mechanism. The quadrotor weighs 388 g and has a payload of 700 g, which must include a battery. After attaching our mechanisms, we witnessed an undesirable amount of independent actuation between the two legs, which caused instability in perching. To combat this, we added two stabilizers (Fig. A.7) connecting the legs on the heel and thigh links. These stabilizers caused the legs to move more dependently, but because of compliance in the joints, the legs can still collapse to slightly different heights, providing the ability to perch on surfaces of different cross-sections. The completed two-leg mechanism weighs 478 g, which is within the payload of the quadrotor and leaves 222 g for batteries and future additions such as cameras or GPS systems. For reference, the 2200 mAh lithium polymer battery we are using weighs 145 g, which means there is 77 g remaining in the payload to add other components; this value will likely need to be increased, which means reducing the weight of the leg will likely be required.

Using the presented analysis and system parameters, it should be possible to predict the largest moment that the system will be able to support on cylindrical perches. Due to the complex behavior of the toes wrapping around a given perch, rather than trying to predict how much each toe segment would deflect, and subsequently how much the tendon would move for a given perch, values were experimentally determined by perching the system on 33 mm and 49 mm diameter rods. δ was found by marking a point on the tendon when the system is fully relaxed, then measuring how far it moved when perched. θ_n was found by taking snapshots of the front and back toes on the perch, then measuring the angles between each link; the values for the front and back were averaged under the assumption that a foot centered on a symmetrical perch would result in equivalent deflections for the front and back toes. The results are summarized in Table 3.2.

Using δ, and looking at Fig. 3.7(a) for $q = 0$ mm, the value of t while perched can be

Table 3.2. Experimental values for toe parameters while perching.

	33 mm Perch	**49 mm Perch**
δ	37 mm	31 mm
θ_1	$(62^\circ + 52^\circ)/2 = 57^\circ$	$(56^\circ + 39^\circ)/2 = 47^\circ$
θ_2	$(60^\circ + 66^\circ)/2 = 63^\circ$	$(51^\circ + 53^\circ)/2 = 52^\circ$
θ_3	$(66^\circ + 71^\circ)/2 = 68^\circ$	$(57^\circ + 61^\circ)/2 = 59^\circ$

determined by addding δ to the initial value (when C_y is largest). Then, using (3.22) and (3.23), C_y and dC_y/dt can be determined. Subsequently, F_a can be determined using (3.19) and F_t using the relationship $F_t = F_a/3$ presented in Chapter 2. Finally, using (3.24)-(3.29), the contact forces on each toe link can be determined. Summing these normal forces, and realizing that there are six similar toes, the maximum moment that can be supported is $M = 6\mu_s r_p \Sigma F_{ci}$. The value of μ_s between the toe and the paint-coated PVC surface used in testing was experimentally found to be 1.47 ± 0.05 by placing a single toe on a flat, paint-coated surface and tilting it through an angle, where $\mu_s = \tan\theta$.

Each of the values necessary for the grip analysis are calculated in Table 3.3. The maximum moment that should be rejected is found to be 1.8 Nm for the 33 mm perch and 2.5 Nm for the 49 mm perch. One area of concern is that the analysis predicts a large negative contact force on the second toe link, which would mean that it is being pulled into the perch. This phenomena does not make physical sense and indicates that there is some flaw in the model. At this time, component level tests have not been conducted to verify the analysis for the leg and foot, which makes it difficult to determine where the problem lies. In an attempt to debug the issues, F_t was manually varied, using the experimental toe deflections in the recursive force calculations (3.24)-(3.29). Additionally, the joint deflections of a single toe were input, and manually varied, using the experimentally calculated F_t. Finally, adjusting the equations such that a negative force is replace by a zero force (since negative forces do not make physical sense) and continuing with the recursive formula, produces the contact forces shown in Table 3.4. None of these procedures produced more logical results, which indicates that the issues may lie in the grip force model. Studying slow-motion video of the joints deflecting while perching shows that link two does not contact the perch for every toe, so it is not surprising that the model does not predict large positive forces, however logically these forces should be predicted to be very close to zero. Furthermore, watching the video indicates that there is some buckling occurring

Table 3.3. Theoretical moment disturbance values. Input parameters are those shown in Table 3.2, $F_w = 533$ g for the rotorcraft and battery, and $\mu_s = 1.47$.

	33 mm Perch	**49 mm Perch**
t	521.9 mm	515.9 mm
C_y	72.3 mm	100.8 mm
dC_y/dt	-4.7 mm/mm	-4.8 mm/mm
F_a	24.7 N	25.0 N
F_t	8.2 N	8.3 N
F_{c1}	13.0 N	13.2 N
F_{c2}	-6.9 N	-8.1 N
F_{c3}	6.3 N	6.4 N
M	1.8 Nm	2.5 Nm

Table 3.4. Theoretical non-negative contact force values. Calculated using the same procedure as that used for Table 3.3, but replacing negative forces with a zero value before proceeding through recursive formula.

	33 mm Perch	**49 mm Perch**
F_{c1}	6.7 N	3.2 N
F_{c2}	0 N	0 N
F_{c3}	6.3 N	6.4 N
M	1.9 Nm	2.1 Nm

at the joints and the pin-joint model based on pure bending may no longer be accurate enough. Additionally, it is possible that the assumption that the contact force is normal to and centered on the link is inaccurate and a better representation of the contact force may lead to improved results. In conclusion, the current toe model seems to accurately predict toe motion through free space, but does not seem to accurately predict contact force in a given perch configuration.

3.4 Experimental System Stability Evaluation

The functional quality of the landing gear was studied through three experiments. First, we studied the ability of the landing gear to support a rotorcraft while perching on a variety of surfaces. Second, we studied the ability of the landing gear to support a rotorcraft under angular perturbations. Third, we studied the ability of the landing gear to support the rotorcraft under horizontal disturbances. Finally, we studied the effects of the rotorcraft landing off-center on the perch. Note that the system was manually placed on the perches as perching from flight is not within the scope of this work.

3.4.1 Versatile Perching Capability

To understand the versatility of the landing gear, the system was perched on a variety of commonly found surfaces. The system is able to perch on many types of surfaces, but performs best on surfaces that allow the toes to contact the item from multiple directions. The cylindrical railing in Fig. 3.12(a) is similar to the PVC tubing used to test the mechanism during development, so it follows that it performs well on this surface. Similarly, the system is able to perch on a tree branch, Fig. 3.12(b), which is roughly cylindrical in shape but is not homogeneous in geometry and texture. Fig. 3.12(c) shows the system perching on a rectangular railing, where the foot is just large enough to grip around the front of the surface; qualitatively, this perch is remarkably stable, and the sharp corners seem to act to lock the toes in place.

On more oddly shaped surfaces, the system can succeed in perching, however its stability is less predictable. For example, Figs. 3.12(d,e) show the system perching on exposed plumbing; the perch shown is stable, however slight angular deviations of the center of mass resulted in

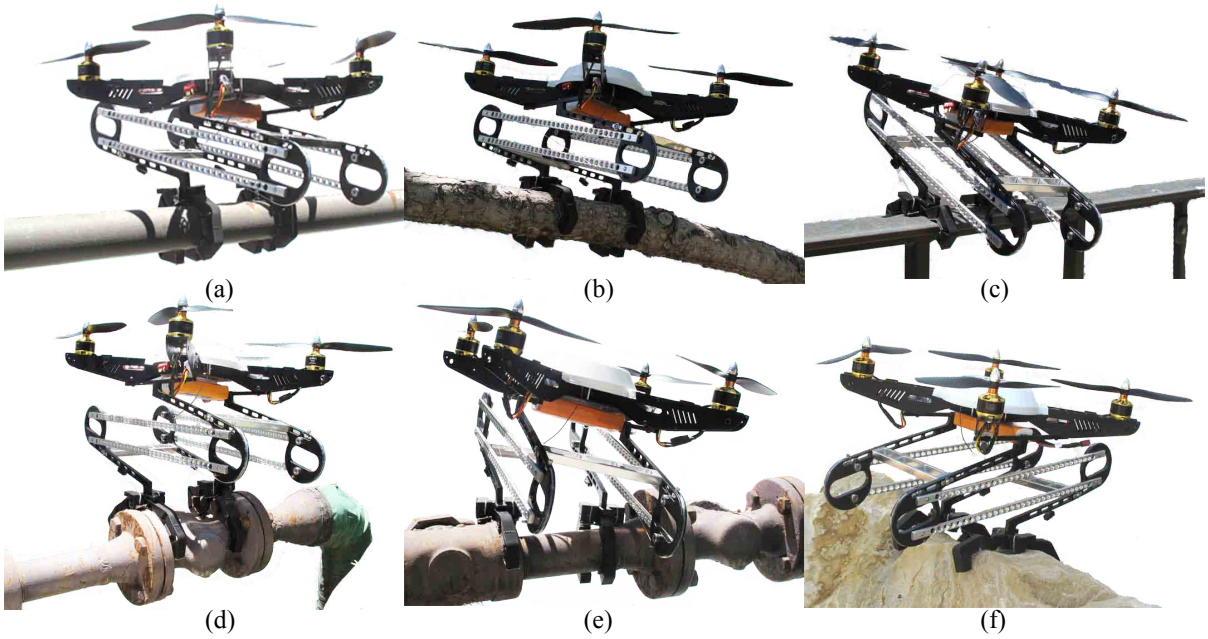

Figure 3.12. Successful perches on common objects. (a) Cylindrical railing. (b) Tree branch. (c) Rectangular railing. (d) Plumbing, with similar foot stances. (e) Plumbing, with asymmetrical foot stances. (f) Ridge of rock.

unstable perches. Notice that the system is not only able to stabilize on perches with uniform foot stance (Fig. 3.12(d)), but also on perches with nonuniform foot stance (Fig. 3.12(e)). Finally, Fig. 3.12(f) shows the system perching on a rock with nonuniform topography.

In addition to perching on common objects, we are interested in how the system lands on flat surfaces. As shown in Fig. 3.13, the legs tilt forward and the system comes to a position resting on the feet and the knee joints. Although this orientation may not be ideal, it is repeatable and stable. The ability of a rotorcraft to take-off from this position will need to be investigated before determining if this in an acceptable landing position. It is possible that changes could be made in leg link lengths to result in a more upright posture when landing on flat surfaces.

3.4.2 Stability Under Angular Perturbations

It is unreasonable to expect a robotic rotorcraft to be able to land on the perch perfectly vertically. As such, we explored the range of angles at which the system is stable. The experimental setup consisted of a perch that was allowed to freely rotate in a v-channel cut into two vertical stands, with an Arduino Mega microcontroller and a GMS high-torque servo motor to control rotation of the perch (Fig. 3.14). With the servo initialized at 0 degrees, the landing mechanism and rotorcraft were centered on the perch; the servo then stepped through rotation in increments of 1 degree and held for 30 seconds. The point at which the landing mechanism

Figure 3.13. Landing on flat ground. The system reaches a stable position resting on the feet and knee joints.

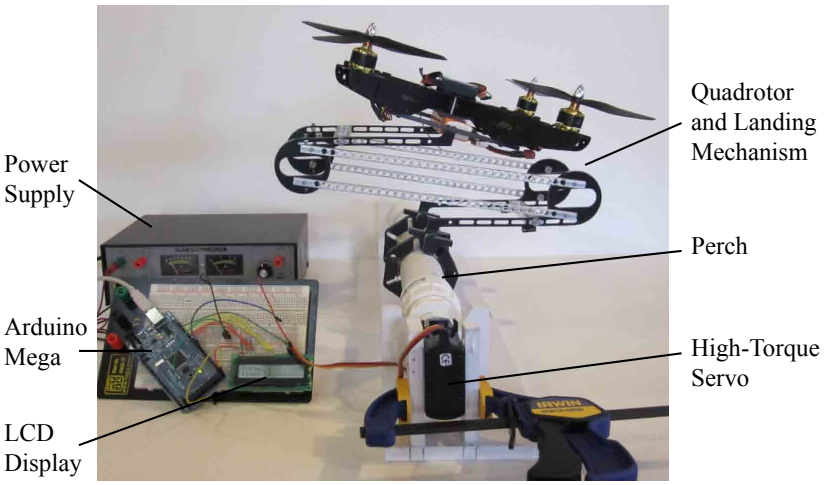

Figure 3.14. Angular perturbation test setup.

released was recorded. Twenty readings were averaged to quantify variance and to reduce error due to initial placement. This method was performed for both positive and negative angles on perches of 33 mm and 49 mm diameters, where a positive angle is defined as one that tilts the front of the rotorcraft toward the ground. The results are summarized in Table 3.5. Equivalent values for the acting moment disturbance are reported in Table 3.6.

There are two important trends to notice from the data. First, the system has a higher tolerance to angular perturbations on the smaller perch; this is because the quadrotor sits

Table 3.5. Angular stability limits. A positive angle is defined as one that tilts the front of the rotorcraft toward the ground.

	33 mm Perch Mean ± StDev	**49 mm Perch** Mean ± StDev
Negative Limit	$-13.5 \pm 1.2°$	$-11.7 \pm 1.3°$
Positive Limit	$11.9 \pm 1.3°$	$9.4 \pm 1.2°$

Table 3.6. Angular stability limits: moment disturbance. The equivalent moment disturbance at the foot can approximately be calculated as the product of the weight of the aircraft, distance of the quadrotor center of mass (COM) above the center of the perch, and the sine of the reported angle in Table 3.5; this neglects the effects of the leg mass. The mass of the quadrotor and battery is 538 g. On the 33 mm perch, the quadrotor COM is 148 mm from the center of the perch. On the 49 mm perch, the quadrotor COM is approximately 191 mm from the center of the perch.

	33 mm Perch Mean ± StDev	**49 mm Perch** Mean ± StDev
Negative Limit	-0.18 ± 0.02 Nm	-0.20 ± 0.02 Nm
Positive Limit	0.16 ± 0.02 Nm	0.17 ± 0.02 Nm

closer to the perch, so the center of gravity produces a smaller moment than on the larger perch. As such, it may be beneficial to determine the most common perch size for a given application, then design the leg so that the aircraft sits low for that size perch. Second, the system has a higher tolerance to angular perturbations in the negative direction; this may be due to the structure of the leg. For instance, when the leg collapses, the shin links are at an angle such that the knee is lower than the ankle; this means that as the aircraft tilts forward (positive angle perturbations) the pitch of the shin links are exaggerated and the center of mass of the leg produces a higher moment. However, when the aircraft tilts backwards (negative angle perturbations), the shin links approach horizontal and the center of mass of the legs produce a lower moment. The data reported here is likely a conservative estimate. As the servo rotated to new positions, at larger angles ($\gtrapprox 10$ degrees) the servo motor was not able to completely overcome the moment imposed on the perch and often sat at a slightly larger angle than that being commanded.

It is important to note that this data is very specific to our given system. For example, two sets of data were collected for angle perturbations on the small perch; one just after stringing the tendons, and a second after pretensioning the tendons so that the quadrotor sat level. The second data set, which is presented in Table 3.5, showed the system to be able to support angle perturbations 2 degrees larger than the first set.

The moments experimentally measured are significantly smaller than those predicted in

Table 3.3. A portion of the decrease in value can be attributed to the fact that when the rotorcraft is perching at an angle, only a portion of the weight is applied to the leg ($F_a = F_w \cos\epsilon$, where ϵ is the angular deviation from vertical). However, for the small angles here, $\cos\epsilon \approx 1$ and the the difference in applied mass is insignificant. As discussed previously, it is likely that the analytical work must be updated to better model the system.

3.4.3 Stability Under Lateral Disturbances

Once the system has made a stable perch, it will likely experience environmental disturbances such as wind. Thus, we designed an experiment to test the amount of horizontal force the system can withstand. The setup from the angular perturbation test was reused, and a pulley was added so that a horizontal force can be applied by hanging weights on a cable, Fig. 3.15. The system was set at angles of 0 degrees and 1/2 the magnitude of the maximum angular perturbation in the positive and negative directions, as reported in Table 3.5. Weight was applied to a cable that was secured to the bottom plate of the quadrotor and held for 30 seconds. The point at which the feet slipped off the perch was recorded. Ten readings were averaged to quantify variance and to reduce error due to initial placement. This method was performed on perches of 33 mm and 49 mm diameters for positive and negative forces, where a positive force is one that acts to move the rotorcraft forward. The results are summarized in Table 3.7. Equivalent values for the acting moment disturbance are reported in Table 3.8.

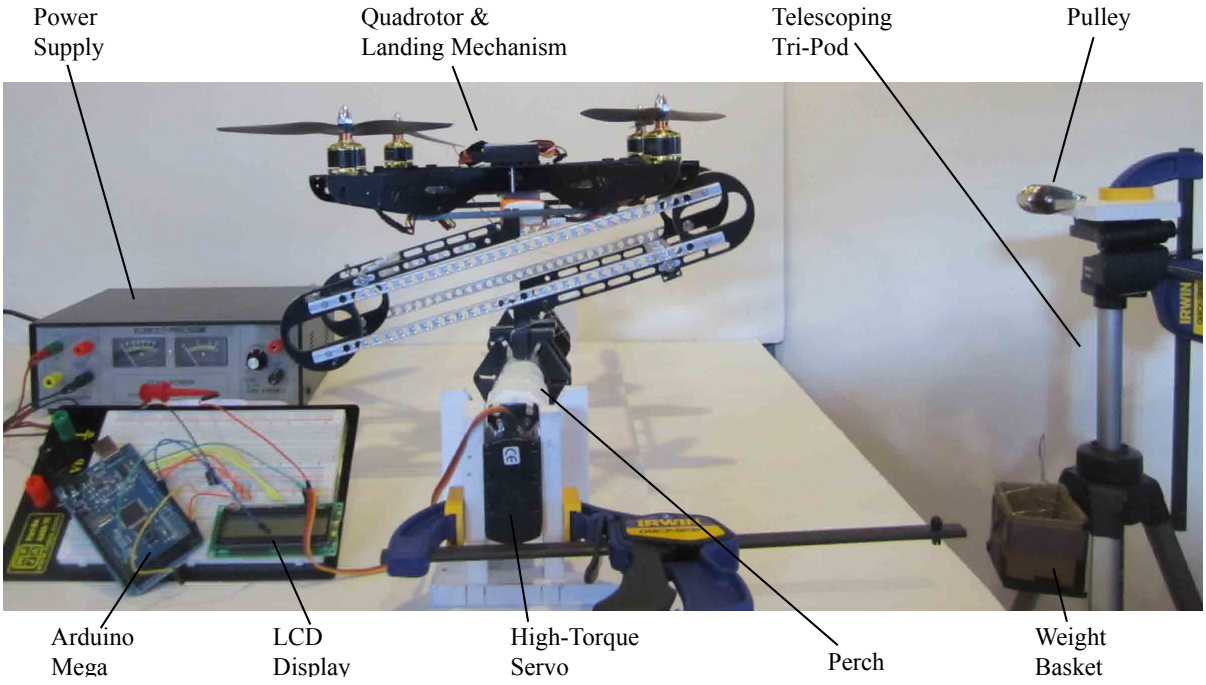

Figure 3.15. Lateral disturbance test setup.

Table 3.7. Lateral force limits. A positive force is one which acts to move the rotorcraft forward.

	33 mm Perch Mean ± StDev		
Perch Angle	**-7 deg**	**0 deg**	**6 deg**
Negative Limit	-1.7 ± 0.1 N	-3.0 ± 0.1 N	-3.7 ± 0.2 N
Positive Limit	3.9 ± 0.2 N	2.6 ± 0.2 N	1.5 ± 0.1 N
	49 mm Perch Mean ± StDev		
Perch Angle	**-6 deg**	**0 deg**	**5 deg**
Negative Limit	-2.1 ± 0.2 N	-3.0 ± 0.2 N	-3.8 ± 0.3 N
Positive Limit	3.5 ± 0.2 N	2.9 ± 0.2 N	1.5 ± 0.2 N

Table 3.8. Lateral force limits: moment disturbance. The equivalent moment disturbance at the foot can be calculated as the product of the reported forces and the distance from the center of the perch at which the force is applied. For the 33 mm perch, the force is applied 137 mm from the center of the perch. For the 49 mm perch, the force is applied 180 mm from the center of the perch.

	33 mm Perch Mean ± StDev		
Perch Angle	**-7 deg**	**0 deg**	**6 deg**
Negative Limit	-0.23 ± 0.02 Nm	-0.40 ± 0.02 Nm	-0.50 ± 0.03 Nm
Positive Limit	0.53 ± 0.02 Nm	0.36 ± 0.02 Nm	0.20 ± 0.01 Nm
	49 mm Perch Mean ± StDev		
Perch Angle	**-6 deg**	**0 deg**	**5 deg**
Negative Limit	-0.37 ± 0.04 Nm	-0.54 ± 0.04 Nm	-0.69 ± 0.05 Nm
Positive Limit	0.62 ± 0.04 Nm	0.52 ± 0.03 Nm	0.27 ± 0.04 Nm

Although a point force is not the same as a wind gust, this data gives an idea of the amount of disturbance that can be supported as it is seen as a moment at the foot. Qualitatively, when a force was applied, the foot flexed at the first joint to accommodate the imposed moment. This continued until the foot was no longer able to grip the perch, at which point it slipped off. This suggests that both grip strength and stiffness of the toe joints are important in determining stability. Quantitatively, there are a number of things to note about the presented data. We will first discuss the data at a 0 degree perch, followed by a discussion of the data at the off-vertical perches.

Perched at 0 degrees, the system is able to support slightly more force in the negative direction than the positive direction. This is likely due to a combination of foot and leg geometry: 1) the foot has one toe in the front and two in the back, so it is reasonable to expect the deflection characteristics of the foot to be asymmetric; and 2) as a force is applied,

the quadrotor body rotates about the foot, and as discussed in the angular perturbation test as the quadrotor tilts forward, the leg is less able to support an applied moment. Furthermore, comparing data at 0 degrees between the two perch sizes, there does not seem to be a significant difference in the amount of force that can be supported. This was unexpected, but it is not unreasonable. We predicted that the bigger perch would be able to support a higher force because it should have a tighter grip that acts around a larger radius, thus producing a higher restoring moment. However, because the quadrotor is sitting higher above the perch, the applied force is also producing a larger moment, so while the applied forces are roughly equal, the applied moments are not, see Table 3.8. Again, the moments experienced are significantly smaller than those predicted in Table 3.3, indicating that the analytical work must be updated to better model the system.

When perched off-vertical, the most obvious thing to notice is that there is an asymmetry between the forces that can be supported in the negative and positive directions. This is as expected. Take, for example, the 33 mm perch at $-7°$: here, a negative force pulls the system in the same direction as gravity and into a larger angle, but a positive force pulls the system against gravity and into a smaller angle. It is tempting to also make a comparison between the positive- and negative-angle data, or between perch sizes, however these would be soft comparisons. Because the angles were selected at half the maximum angle perturbation found previously, each data set should correspond to a similar stability region (and as such have similar results), but an exact comparison shouldn't be made.

3.4.4 Stability Under Lateral Displacement

In an attempt to understand how the system would act if the rotorcraft lands such that the perch is not centered in the palm, we devised an experiment where the quadrotor is hung from a string and lowered on to the perch to simulate flight, as seen in Fig. 3.16. As the rotorcraft hung from the strings, it was difficult to stabilize the motion so that the body did not sway or rotate while lowering. As a result, we do not have quantitative results to report, but will discuss the results qualitatively.

It was relatively difficult to stabilize the rotorcraft on a perch by lowering it on strings. As the leg began to collapse, the rotorcraft began to tip forward or backwards, not allowing grasp to be made. Occasionally, a grip was made if the rotorcraft was centered well on the perch. These results are supported by a quick analysis of the stable perching angles. For the 49 mm perch, the rotorcraft has a stable perch at angles $-11.7° < \alpha < 9.4°$; the corresponding lateral displacement from center is $R \tan \alpha$ or -5 mm $< x <$ 4 mm. This is a very small range, and as such was hard to hit accurately using this test setup. It is likely that the test can only be accurately conducted after a flight algorithm has been developed, because any apparatus

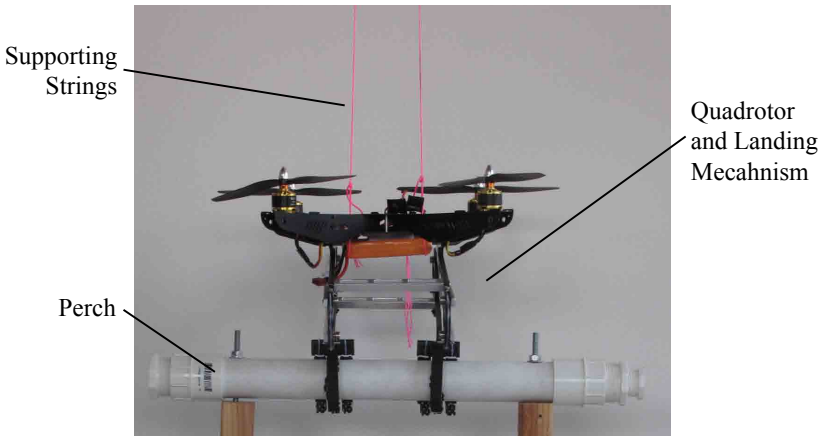

Figure 3.16. Lateral displacement test setup.

designed to constrain the undesirable sway of our setup would also exert forces that would not exist in flight.

3.5 Conclusions

The prototype presented in this chapter provides a vast improvement over our previous design. As a stand-alone mechanism, it is qualitatively more stable than the previous design and provides a more predictable behavior and a better life-cycle. After attaching two legs to a quadrotor, versatility tests were conducted that showed the system is able to perch on a number of different surfaces. Additionally, stability tests demonstrated the range of moment disturbances that can be supported. These results demonstrate that passive perching on a variety or surfaces is possible.

Although this current prototype performs well, improvements can be made in future design iterations. One topic of interest is studying the effects of altering toe length and the number of segments; it is possible that better grips on a wider variety of surfaces can be achieved by altering these characteristics. Also, the current prototype dimensions were chosen somewhat arbitrarily so that the mechanism was scaled to the size of a quadrotor and achieved at least the minimum tendon pull and tension necessary to close the foot; using the presented analysis, more optimal dimensions can be selected to reduce weight and improve performance.

CHAPTER 4

CONCLUSIONS AND FUTURE WORK

The purpose of this thesis is to develop an avian-inspired mechanism that enables a rotorcraft to perch on a variety of surfaces. The concept integrates a compliant, tendon-driven, underactuated gripper with a leg mechanism that converts rotorcraft weight into an applied tension at the foot. Two prototype iterations were discussed, including the design and analysis of the components. Functional and stability tests were performed on the second prototype and the results are promising. The landing gear, attached to a quadrotor, was shown to be capable of perching on a variety of surfaces such as round shapes, rectangular shapes, and nonuniform surfaces. The mechanism reaches a repeatable and stable position on flat ground, although the quadrotor sits at an angle. The stability tests show that the system can withstand reasonable moments, and can likely be improved upon in further design iterations.

The presented prototypes show that the concept of avian-inspired passive perching is achievable; the design, however, is not yet optimal. Suggested topics for future work are listed and discussed here.

- *Leg Size*: Most of the dimensions used to manufacture the leg were chosen somewhat arbitrarily, provided they met the necessary requirements for force and tendon displacement to close the toes. Using the presented analysis, more optimal dimensions should be chosen for weight reduction and better performance. It is possible that better performance on flat ground is achievable by adjusting the link lengths.

- *Shin Dimensions*: Currently, two mechanical pin-type stops are used to restrain the motion of the leg when freely dangling beneath the rotorcraft. Rather than using a dedicated component to achieve this mechanical stop, the dimension p between the two shin links can be adjusted so that the links stop on each other at a desired angle. Adjusting p will also change how low the aircraft can sit above a perch, as the current shin configuration hits the quadrotor base on small perches.

- *Leg and Toe Material*: The materials used to construct the leg and were mainly selected for convenience. Lighter materials are available and should be considered in future iterations.

- *Toe Links*: The toes used in the prototypes were developed using high-level concepts that demonstrated an appropriate pattern for joint stiffness (proximal joints stiffer than distal

joints); the link lengths and quantity, however, were chosen arbitrarily. The landing gear would benefit by studying the effects of changing link lengths and numbers. For example, perching birds have a different number of links in each toe, one in the back and two, three, and four in the front [13]; it is possible that our mechanism would benefit from a similar characteristic. Also, changing link lengths may improve the range of objects that can be perched on. Finally,adding a pre-curve to the toe to reduce the sag under its own weight could be considered.

- *Toe Pads*: The material used on the contact surface of the toes would likely benefit from further research. The materials used currently have a tendency to shear off when supporting large moments on the perch. This is undesirable and must be improved upon before the mechanism can be utilized in practical applications.

- *Toe Manufacturing*: The current process for assembling the toes is not appropriate as a long-term design. The tubing is adhered to the toe via staples, which is a laborious and non-exact process. It is not unreasonable to expect that a molding process would be desirable, similar to [34], and could even allow for a combination of materials for better performance.

- *Tendon Tensioning*: A quick design using a screw and lock nut was utilized to allow for adjustable tensioning of the tendon. The set-up, however, is not easy to use, as the slick tendon material has a tendency to unwrap from the screw if not properly secured, or to be cut by the screw threads if tightened too much. One possible solution would be to replace the current screw with one where the threads are removed at the top and a through-hole is drilled in the shaft, similar to a tuning peg on a guitar.

- *Further Testing*: High-level functional testing was completed to show that the system is stable under reasonable conditions. However, a full analysis of the system predicts a better ability to resist moments than actually experienced. The work would benefit from component level tests that would indicate the models that need more refinement.

- *Flight Dynamics*: The current design was developed with minimal consideration for flight dynamics. Although designed to be within the payload capacity of the quadrotor, the aerodynamics of the system have not been studied. This is an important step to be considered for a practical device. It is possible that an additional mechanism will be required that will lock the leg in a collapsed position during flight to reduce the effects on flight.

- *Additional Applications*: It is likely, through minor changes or additions, that this mechanism can be used for applications beyond versatile rotorcraft perching. For example,

securing the tendon to a motor, rather than the top of the leg, would enable for grasping objects in flight. Additionally, making the orientation of the leg variable might allow for the mechanism to be used on aircraft not capable of vertical landing or take-off.

APPENDIX

SOLIDWORKS MODELS

This appendix includes engineering drawings of each of the manufactured components of the landing gear. Also included are the sub-assemblies (foot and single leg) and finally a drawing of the completed system. Figs. A.4-A.8 were created based on the designs developed by the senior design team, and updated to reflect the final mechanism.

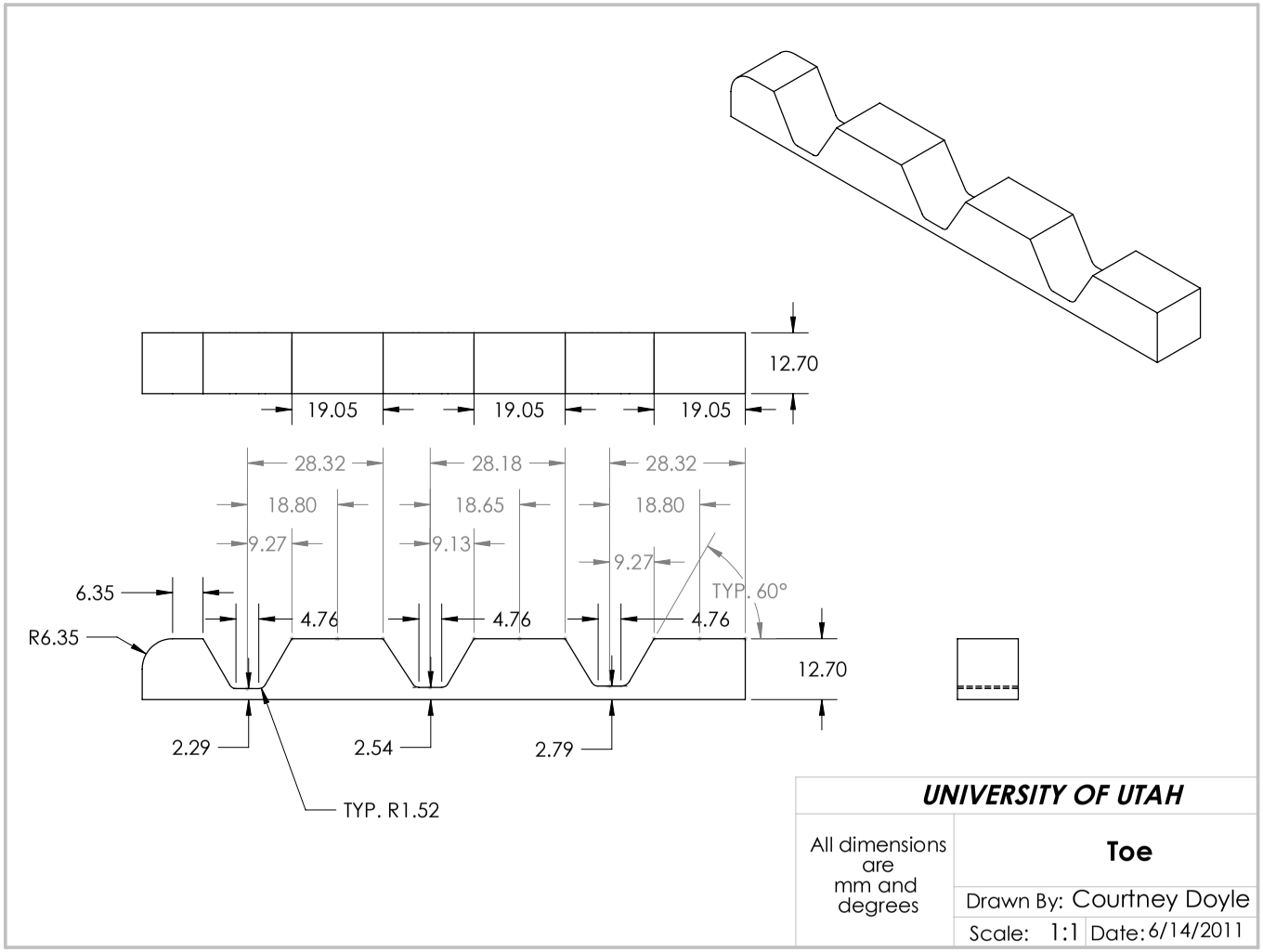

Figure A.1. Drawing of toe.

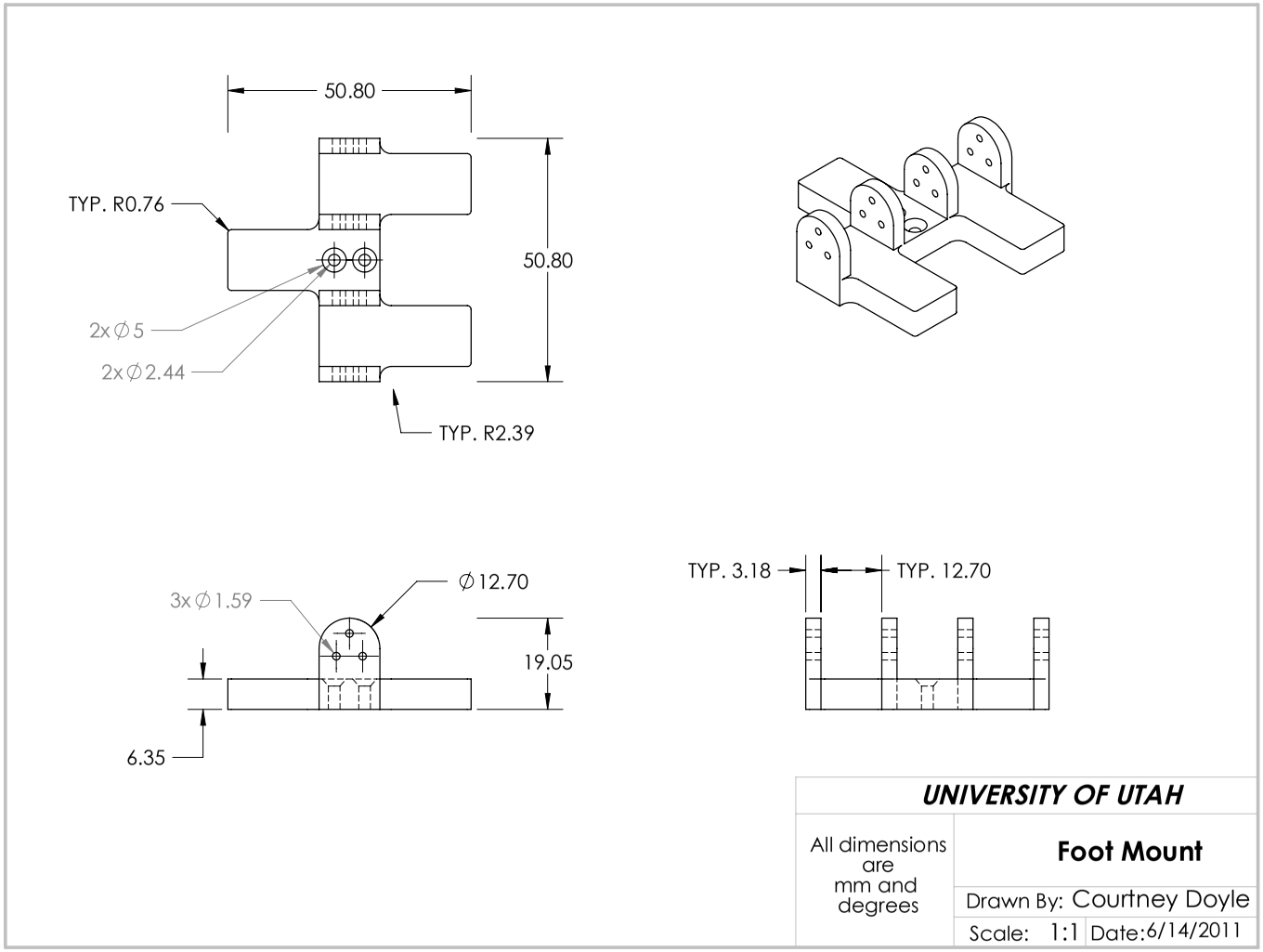

Figure A.2. Drawing of foot mount.

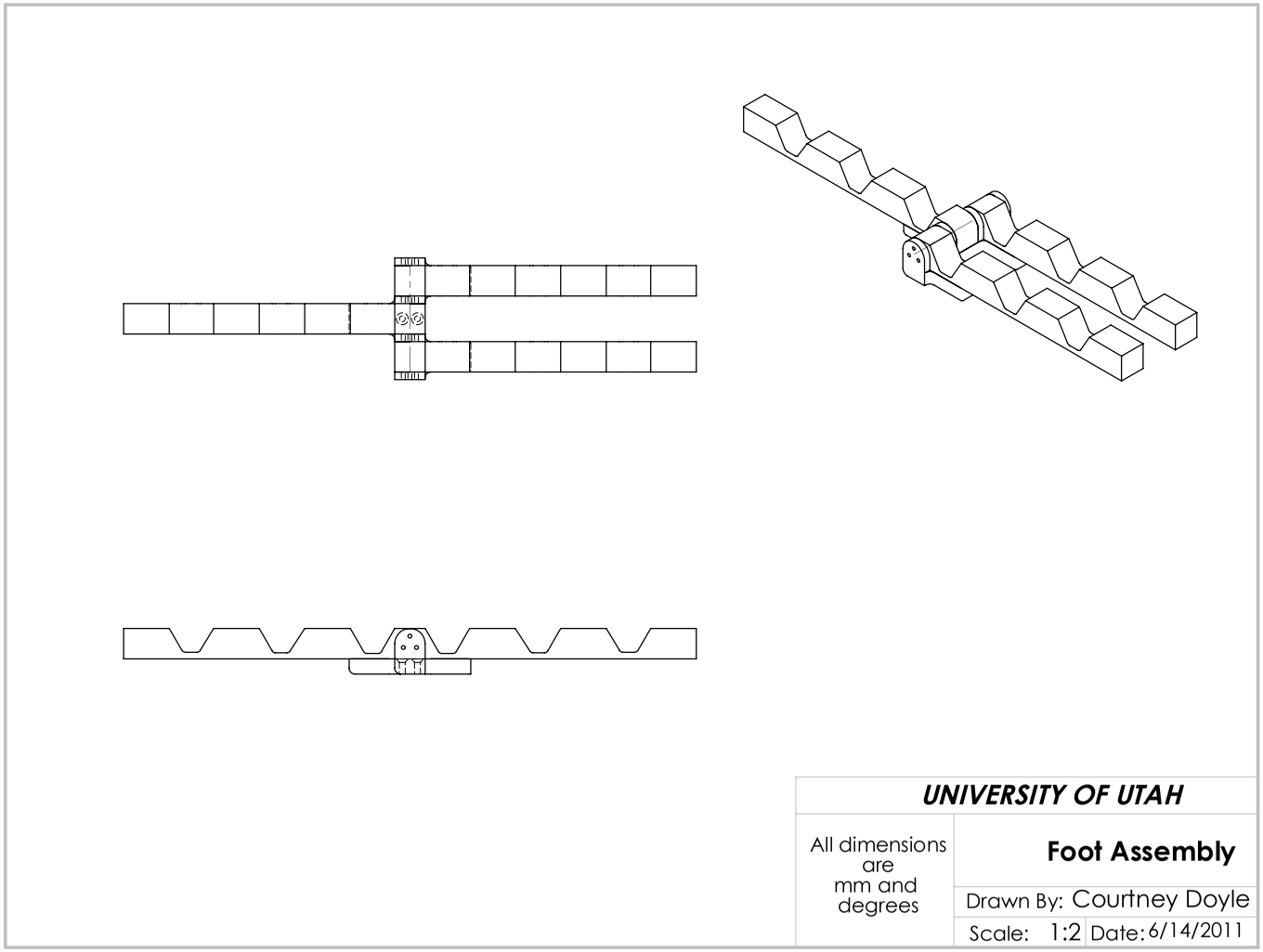

Figure A.3. Assembly drawing of foot.

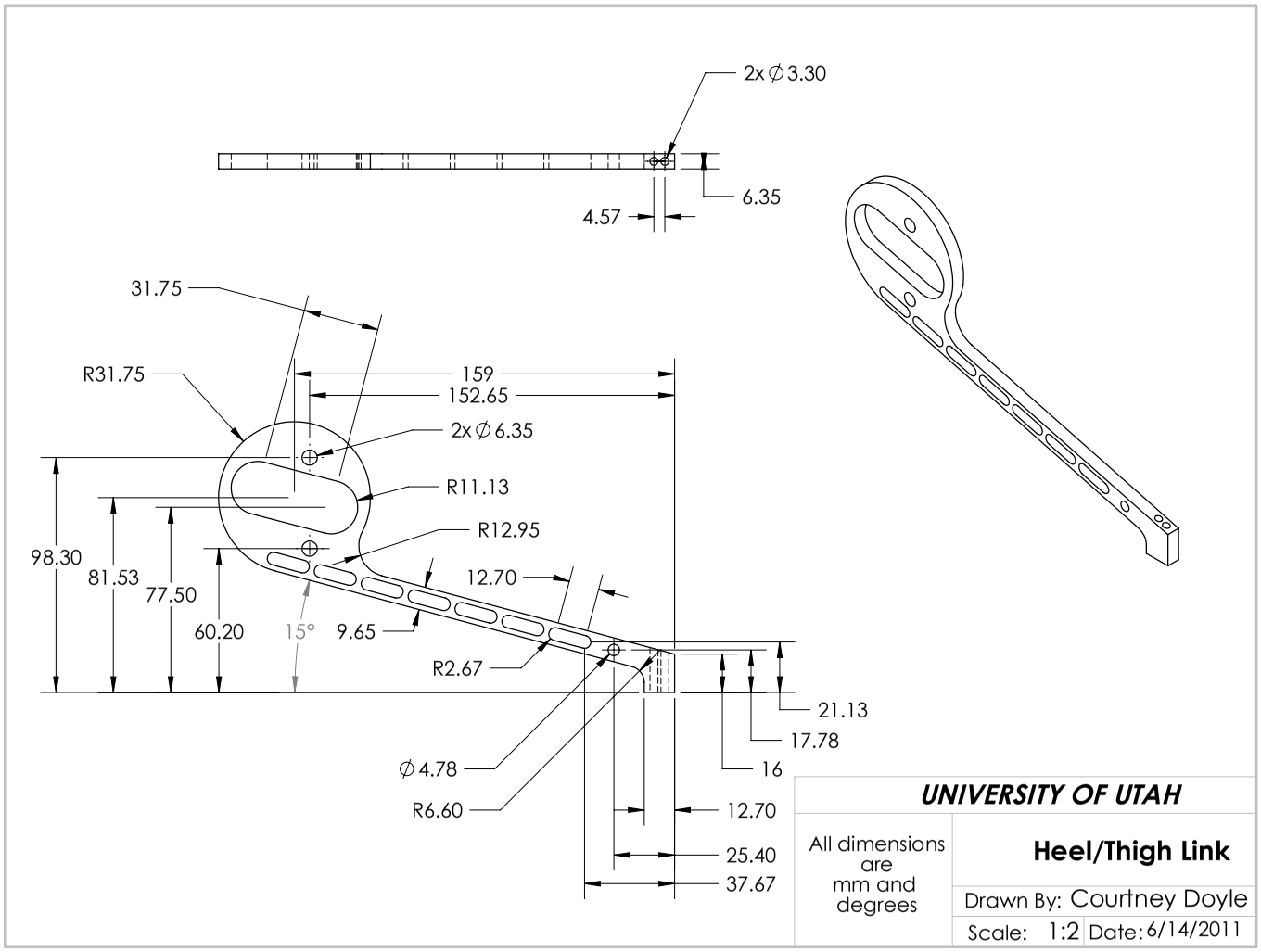

Figure A.4. Drawing of heel/thigh.

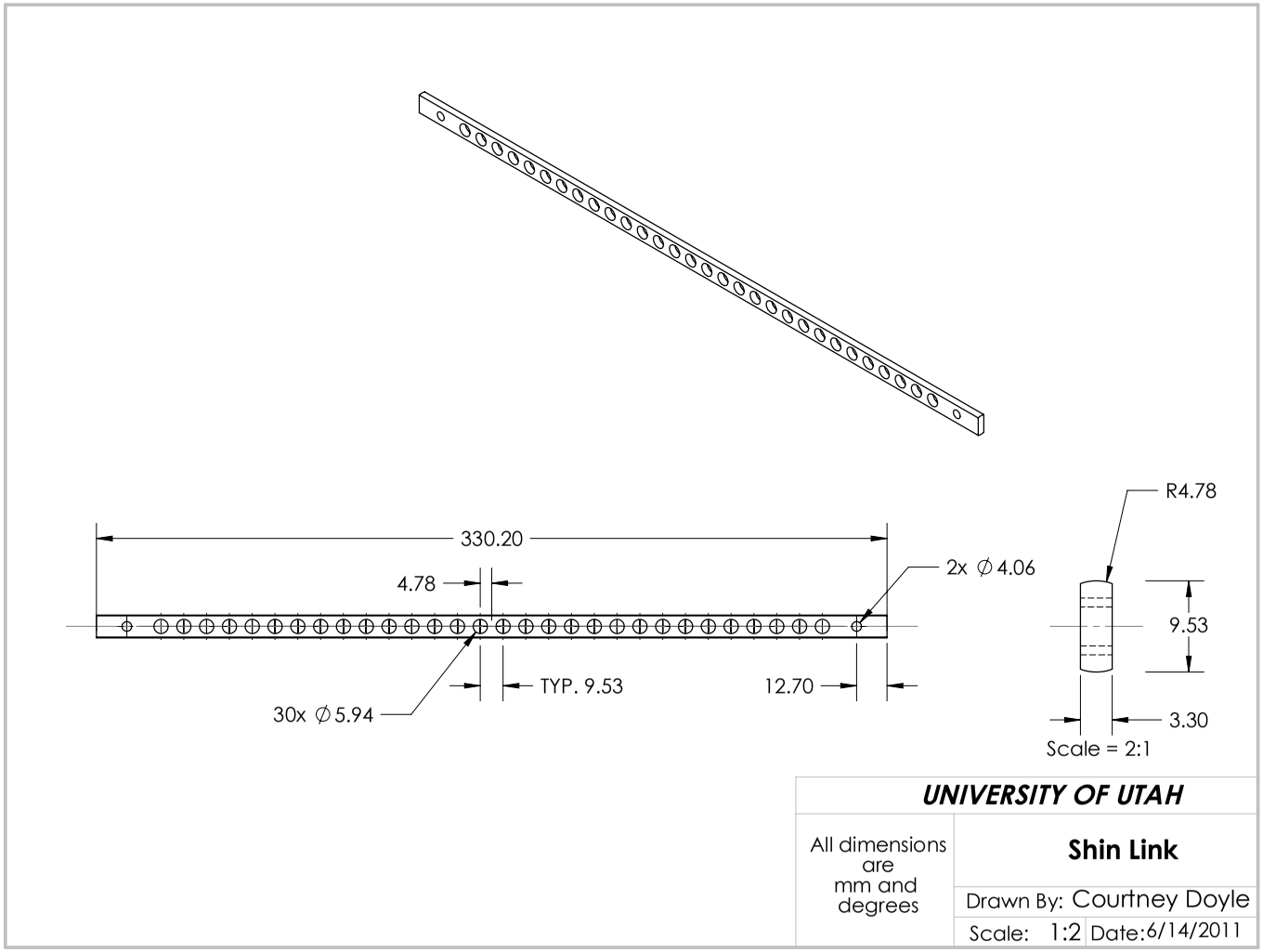

Figure A.5. Drawing of shin.

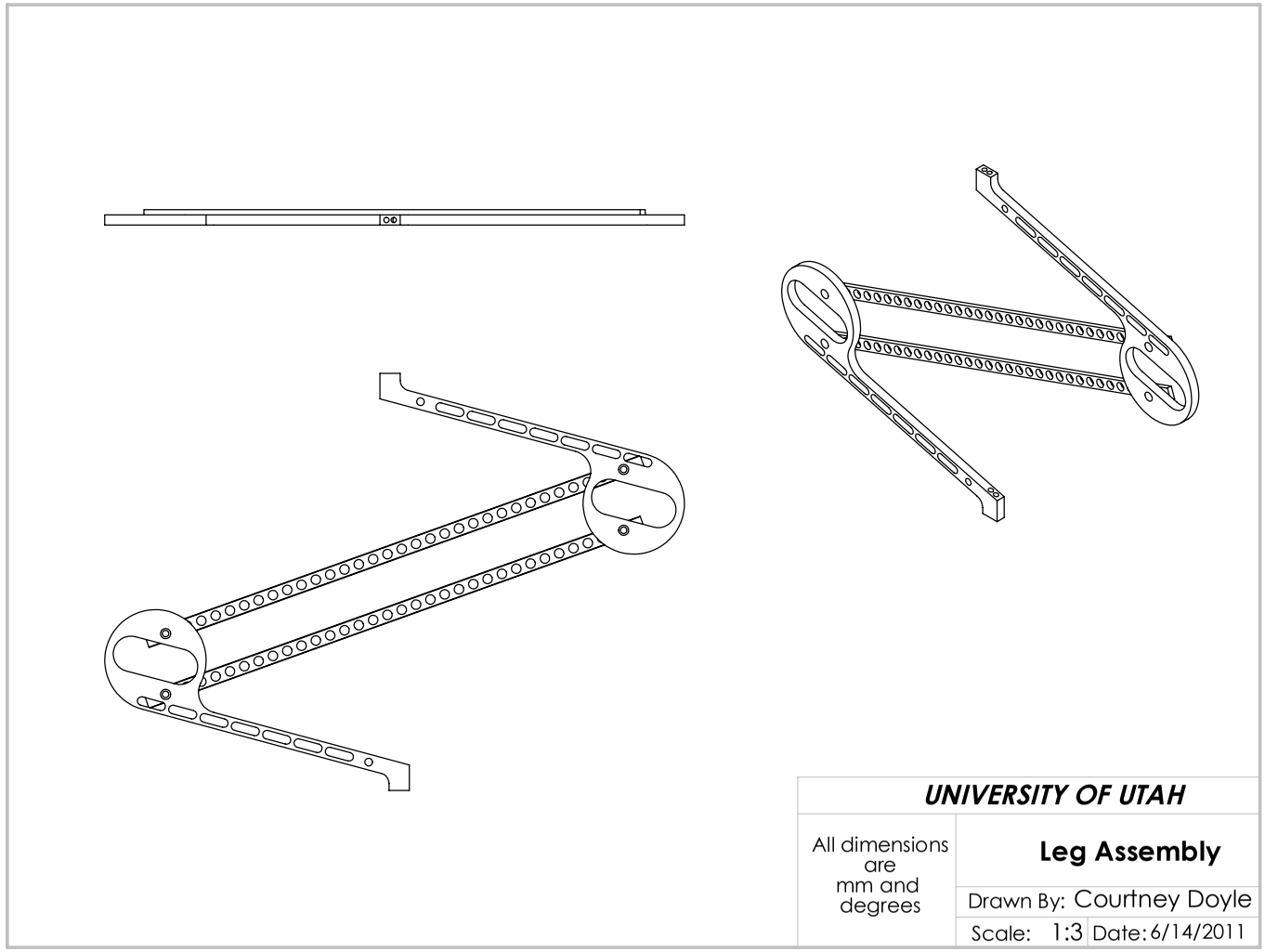

Figure A.6. Assembly drawing of leg.

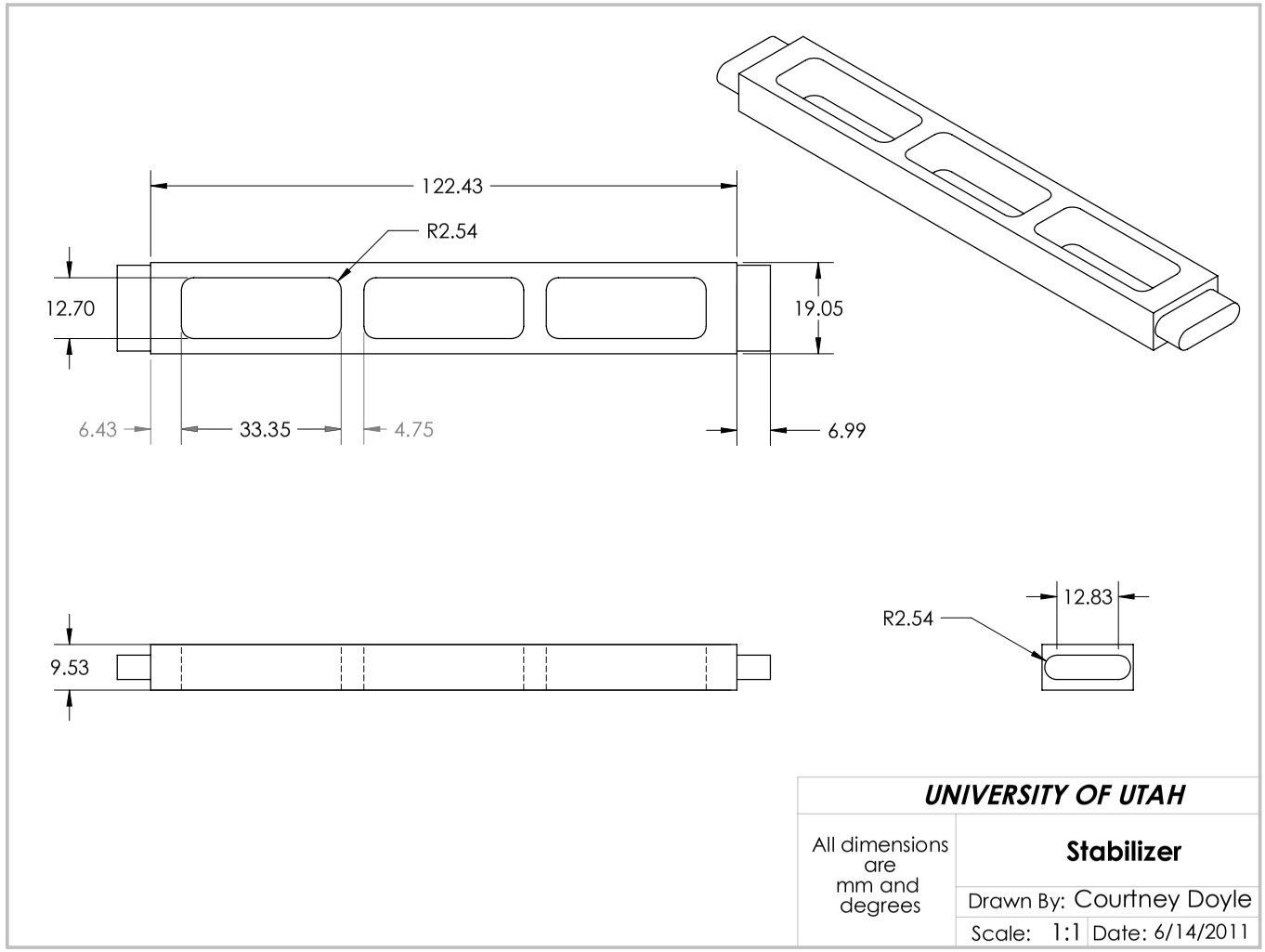

Figure A.7. Drawing of stabilizer.

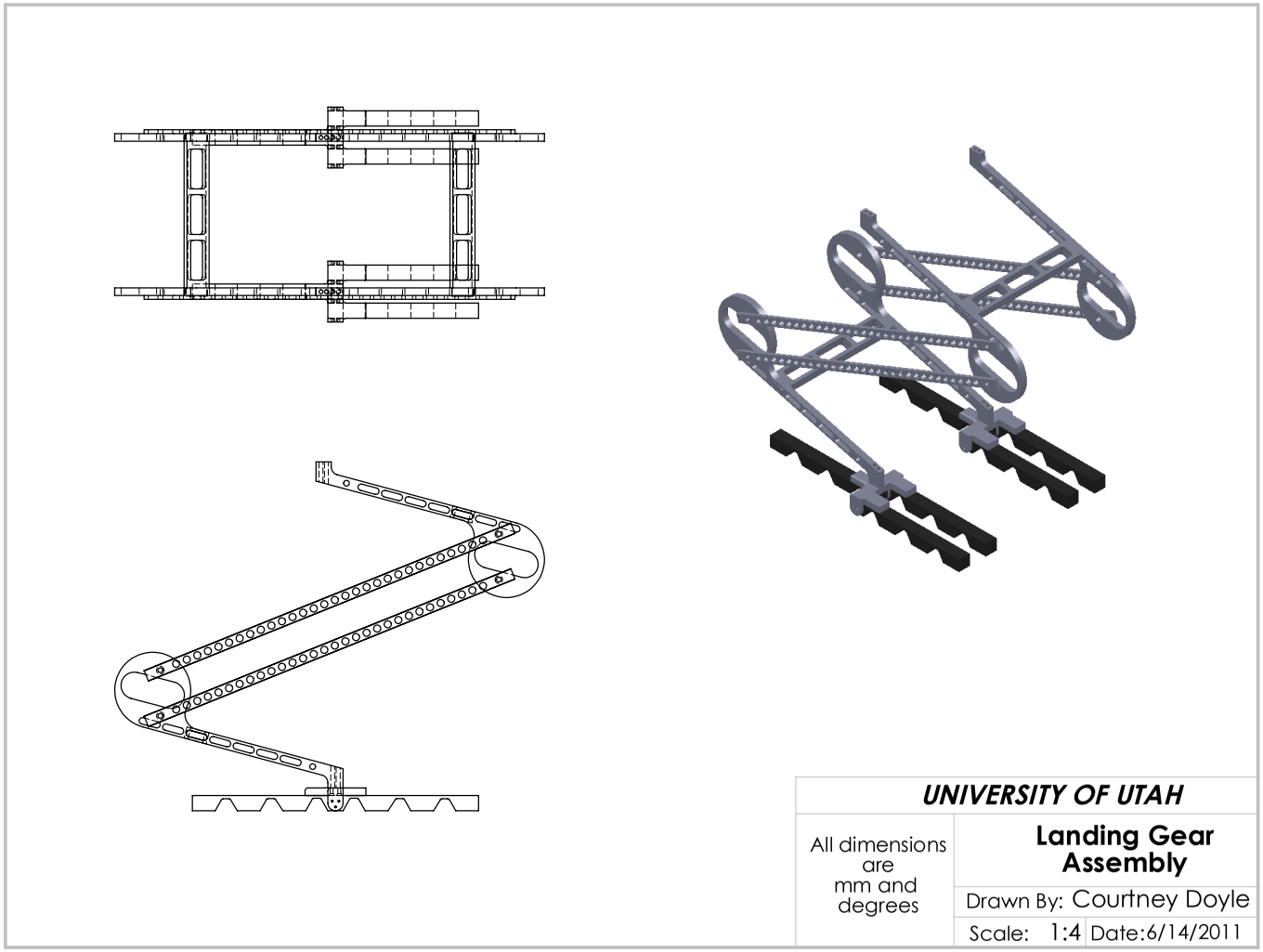

Figure A.8. Assembly drawing of entire system.

REFERENCES

[1] R. Cory and R. Tedrake, "Experiments in fixed-wing UAV perching," in *Proc. AIAA Guidance, Navigation, and Control Conf.*, 2008, pp. 1–12.

[2] A. L. Desbiens, A. T. Asbeck, and M. R. Cutkosky, "Landing, perching and taking off from vertical surfaces," *Int. J. Robotics Research*, vol. 30, no. 3, pp. 355–370, 2011.

[3] D. Mellinger, M. Shomin, and V. Kumar, "Control of quatrotors for robust perching and landing," in *Proc. Int. Powered Lift Conf.*, 2010.

[4] A. M. Wickenheiser and E. Garcia, "Longitudinal dynamics of a perching aircraft," *J. Aircraft*, vol. 43, no. 5, pp. 1386–1392, 2006.

[5] ——, "Optimization of perching maneuvers through vehicle morphing," *J. Guidance, Control, and Dynamics*, vol. 31, no. 4, pp. 815–823, 2008.

[6] R. J. Bachmann, F. J. Boria, P. G. Ifju, R. D. Quinn, J. E. Kline, and R. Vaidyanathan, "Utility of a sensor platform capable of aerial and terrestrial locomotion," in *Proc. IEEE/ASME Int. Conf. Advanced Intelligent Mechatronics*, 2005, pp. 1581–1586.

[7] R. J. Bachmann, F. J. Boria, R. Vaidyanathan, P. G. Ifju, and R. D. Quinn, "A biologically inspired micro-vehicle capable of aerial and terrestrial locomotion," *Mechanism and Machine Theory*, vol. 44, pp. 513–526, 2009.

[8] P. Abbeel, A. Coates, M. Quigley, and A. Y. Ng, "An application of reinforcement learning to aerobatic helicopter flight," in *Advances in Neural Information Processing Systems*, 2007.

[9] D. Mellinger, M. Shomin, and V. Kumar, "Trajectory generation and control for precise aggressive maneuvers with quadrotors," in *Proc. Int. Symp. on Experimental Robotics*, 2010.

[10] T. W. Danko, A. Kellas, and P. Y. Oh, "Robotic rotorcraft and perch-and-stare: Sensing landing zones and handling obscurants," in *Proc. IEEE Int. Conf. Advanced Robotics*, 2005, pp. 296–302.

[11] A. Bachrach, R. He, and N. Roy, "Autonomous flight in unknown indoor environments," *Int. J. Micro Air Vehicles*, vol. 1, pp. 217–228, 2009.

[12] E. Britannica. (2011) Bird. [Online]. Available: http://www.britannica.com/EBchecked/topic/66391/bird

[13] N. S. Proctor and P. J. Lynch, *Manual of Ornithology: Avian Structure and Function.* Ann Arbor, Michigan: Edwards Brothers, Inc., 1993.

[14] F. B. Gill, *Ornithology*, 3rd ed. New York: W. H. Freeman and Company, 2007.

[15] A. M. Ramos and I. D. Walker, "Raptors—inroads to multifingered grasping," in *Proc. IEEE/RSJ Int. Conf. Intelligent Robots and Systems*, 1998, pp. 467–475.

[16] A. M. Ramos, I. A. Gravagne, and I. D. Walker, "Goldfinger: A non-anthropomorphic, dextrous robot hand," in *Proc. IEEE Int. Conf. Robotics and Automation*, 1999, pp. 913–919.

[17] S. Hirose and Y. Umetani, "The development of soft gripper for the versatile robot hand," *Mechanism and Machine Theory*, vol. 3, pp. 351–359, 1978.

[18] J. D. Crisman, C. Kanojia, and I. Zeid, "Graspar: A flexible, easily controllable robotic hand," *IEEE Robotics and Automations Mag.*, vol. 3, no. 2, pp. 32–38, 1996.

[19] C. Gosselin, F. Pelletier, and T. Laliberté, "An anthropomorphic underactuated robotic hand with 15 dofs and a single actuator," in *Proc. IEEE Int. Conf. Robotics and Automation*, 2008, pp. 749–754.

[20] B. Massa, S. Roccella, M. C. Carrozza, and P. Dario, "Design and development of an underactuated prosthetic hand," in *Proc. IEEE Int. Conf. Robotics and Automation*, 2002, pp. 3374–3379.

[21] C. Cho, Y. Lee, and M. Kim, "Underactuated hand with passive adaptation," in *Proc. IEEE Int. Symp. Industrial Electronics*, 2009, pp. 995–1000.

[22] A. M. Dollar and R. D. Howe, "The highly adaptive SDM hand: Design and performance evaluation," *Int. J. Robotics Research*, vol. 29, pp. 585–597, 2010.

[23] T. Laliberté, L. Birglen, and C. M. Gosselin, "Underactuation in robotic grasping hands," *Machine Intelligence and Robotic Control*, vol. 4, no. 3, pp. 1–11, 2002.

[24] M. Luo, T. Mei, X. Wang, and Y. Yu, "Grasp characteristics of an underactuated robot hand," in *Proc. IEEE Int. Conf. Robotics and Automation*, vol. 3, 2004.

[25] M. Doria and L. Birglen, "Design of an underactuated compliant gripper for surgery using nitinol," *J. Med. Devices*, vol. 3, no. 011007, 2009.

[26] B. Almasri and F. B. Ouezdou, "New design of one motor driven under actuated humanoid hand," in *Proc. IEEE/RSJ Int. Conf. Intelligent Robots and Systems*, 2007, pp. 1491–1496.

[27] Y. Liu, A. Hoover, and I. Walker, "Dynamic intercept and manipulation of objects using a novel pneumatic robot hand," in *Proc. Int. Conf. Advanced Robotics*, 2005, pp. 129–134.

[28] D. Trivedi, C. D. Rahn, W. M. Kier, and I. D. Walker, "Soft robotics: Biological inspiration, state of the art, and future research," *Applied Bionics and Biomechanics*, vol. 5, no. 3, pp. 99–117, 2008.

[29] P. E. I. Pounds and A. M. Dollar, "Hovering stability of helicopters with elastic constraints," in *Proc. ASME Dynamics Systems and Control Conf.*, 2010.

[30] C. E. Doyle, J. J. Bird, T. A. Isom, C. J. Johnson, J. C. Kallman, J. A. Simpson, R. J. King, J. J. Abbott, and M. A. Minor, "Avian-inspired passive perching mechanism for robotic rotorcraft," in *Proc. IEEE/RSJ Int. Conf. Intelligent Robots and Systems*, 2011, pp. 4975–4980.

[31] C. E. Doyle, J. J. Bird, T. A. Isom, J. C. Kallman, R. J. King, D. F. Bareiss, D. J. Dunlop, J. J. Abbott, and M. A. Minor, "An avian-inspired passive mechanism for quadrotor perching," *IEEE/ASME Trans. Mechatronics (submitted)*, 2012.

[32] L. L. Howell, *Compliant Mechanisms*, 1st ed. New York: John Wiley & Sons, Inc., 2001.

[33] L. Birglen and C. M. Gosselin, "Kinetostatic analysis of underactuated fingers," *IEEE Trans. Robotics and Automation*, vol. 20, no. 2, pp. 211–221, 2004.

[34] A. M. Dollar and R. D. Howe, "A robust compliant grasper via shape deposition manufacturing," *IEEE/ASME Trans. Mechatronics*, vol. 11, no. 2, pp. 154–161, 2006.